J. Earth Syst. Sci. (2020) 129:29
https://doi.org/10.1007/s12040-019-1276-5

Elucidating intra-seasonal characteristics of Indian summer monsoon. Part-I: Viewed from remote sensing observations, reanalysis and model datasets

Dipak K Sahu[1,3,*], T N Krishnamurti[1] and Vinay Kumar[2]

[1]*Department of Earth, Ocean and Atmospheric Sciences, Florida State University, Tallahassee, FL 32306, USA.*
[2]*Department of Environmental Engineering, Texas A&M University, Kingsville, TX 78363, USA.*
[3]*Present address: RMSI Pvt. Ltd., A-8, Sector-16, Noida, Uttar Pradesh 201301, India.*
**Corresponding author. e-mail: dsahu@fsu.edu dipakmath@gmail.com*

MS received 22 September 2017; revised 23 April 2019; accepted 3 August 2019; published online 20 December 2019

In this study, we examine the transitions in the monsoon phases (onset, active, break and the withdrawal) during an entire monsoon season. This makes use of a host of observational tools that come from GPM (Global Precipitation Measurement) and TRMM (Tropical Rainfall Measuring Mission) satellites for precipitation estimates, the vertical structure of rain, hydrometeors and cloud types from TRMM and CloudSat datasets. During onset, the mean moisture convergence, especially over west and south-west coast of India is 2×10^{-4} kg m^{-1} s^{-1}; however, it carries much higher value of $>4 \times 10^{-4}$ kg m^{-1} s^{-1} during the active phase over central eastern India. Much lesser moisture convergence ($<1 \times 10^{-4}$ kg m^{-1} s^{-1}) is noted over Western Ghats area during the break phase. However, there are northeasterly moisture fluxes present over southern part of India during withdrawal phase. The tall cumulonimbus clouds that extend out to 16 km are illustrate during onset, the active phase is dominated by alto stratus and nimbostratus type clouds that are somewhat shallower. In general, we noted an absence of such clouds during the break and the withdrawal phases. Those structures were consistent in a number of derived fields such as the moisture convergence, moisture fluxes, the energy conversions between the rotational and the divergent kinetic energy and the corresponding phases of the intra-seasonal oscillations.

Keywords. Intra-seasonal phases of the monsoon; structure of the monsoon; kinematic and dynamical features of the monsoon phases.

1. Introduction

This is a two-part study on the structure and mechanisms that control the intra-seasonal phases of an entire summer monsoon season. The monsoon phases relate to the following: the onset, active, break, revival and the withdrawal, of summer monsoon over South Asia covering an entire season. This two-part study is a sequel to an earlier study, Krishnamurti and Biswas (2006), on the transitions of the surface energy balance during the life cycle of an entire monsoon season. The working definitions of the monsoon phases have been described in Rao (1976). India Meteorological Department (http://www.imd.gov.in) prepares the dates of these phases on an annual basis from the surface rain-gauge based rainfall estimates. There are currently close to 2500 rain-gauge sites well distributed all over India (Rajeevan *et al.* 2005) that provide precipitation estimates on a daily

basis. In recent several studies, Roja Raman *et al.* (2008), Deshpande and Goswami (2014), Sahu *et al.* (2014) and Revadekar *et al.* (2016) address the relationships between intra-seasonal monsoon variability and the rainfall pattern, heavy rainfall events, atmospheric circulation, and various components of atmosphere over Indian region. The study conducted by Deshpande and Goswami (2014) described the diurnal cycle of the rainfall over India significantly affected by the active and break phases of the Indian summer monsoon rainfall. Their study shows that there was delay in the occurrence of the afternoon peak in the rainfall intensity over central India during break phases of monsoon. Roja Raman *et al.* (2008) discussed the variation of the Hadley cell with the monsoon activity from the Gadanki mesosphere, stratosphere, and troposphere (MST) radar observations. Their study noticed that the Hadley cell extend towards north during active monsoon phases, and it extends towards south during the break phases. Sahu *et al.* (2014) address a couple of heavy rainfall events over north India associated with the active phases of Indian summer monsoon and their modelling study. During heavy rainfall events, large magnitude of the heat content anomaly excites the thermodynamical wave trains (Krishnamurti *et al.* 2016). This wave train carries large amount of heat from monsoonal region to the Arctic Ice region. Revadekar *et al.* (2016) discuss the distributions of CO_2 over Indian region in response to the atmospheric circulations during active and break phases of Indian summer monsoon. Their study illustrated that anomalous circulation pattern during active and break phases of monsoon, which shows resemblance with high and low values of CO_2. Many of the studies describe the role of cloud microphysics and net annual radiation budget, but not for the monsoonal cycle (Wonsick *et al.* 2009; Hazra *et al.* 2017). Further, some of the studies considered only a few aspects of active and break of the monsoonal cycle, to understand the characteristics of the clouds and their interaction with circulation and convection (Krishnamurti and Kishtawal 2000; Kiran *et al.* 2009; Pillai and Sahai 2014). The present study carries out a complete diagnostic analysis of most of the physical and thermodynamic variables to describe the intra-seasonal variability of the Indian summer monsoon (onset, active, break and withdrawal).

Figure 1 shows the daily averaged all India rainfall during the 2014 summer monsoon season (that extends from June to September). The present study examines the vertical structures of clouds and cloud types that dominate during these monsoon phases and how they impact the differences in the surface energy balance during a monsoon season. The present study also addresses the ψ (stream function)–χ (velocity potential) interactions during the transition of monsoon phases. In the previous study, Krishnamurti and Biswas (2006) noted that the pre-onset phase was quite different from the break phase of moisture. That was largely in the prolonged dryness of the pre-onset phase and the large retention of soil moisture during the break phases that followed an active (rainfall) phase. The role of clouds or cloud types was not addressed in that previous study. Cloud radiation impacts the surface temperature and the long wave radiation alters the surface energy balance, hence the prevailing cloud structures during the monsoon phases are quite important. This new study utilizes vertical structures from a host of recent satellite datasets, those include the Tropical Rainfall Measuring Mission (TRMM) precipitation radar, the global constellation of satellites Precipitation Measurement Missions/Global Precipitation Measurement (PMM/GPM) and the GPM radar, and cloud structure datasets from CloudSat. A number of kinematic and dynamical fields that exhibit large transitions from one phase to the next are illustrated. The phases of the monsoon were known for nearly 100 years (Rao 1976). These phases have now been linked to intra-seasonal oscillations (Waliser *et al.* 2003; Waliser 2006; Kulkarni *et al.* 2011). Chakraborty and Nanjundiah (2012) noted that a strong linear relationship is obtained between the center/scale of convective wave bands and intensity of monsoon precipitation over Indian land on the inter-annual time scale. In part 1 of this study, we display and discuss several local features over South Asia for these respective phases. Part 2 of this study is on the remote teleconnections of the monsoon rainfall variability on the intra-seasonal time scale as it relates to remote forcing such as MJO (Madden–Julian Oscillation), PDO (Pacific Decadal Oscillation), NAO (North Atlantic Oscillation), Eurasian snow and ice cover and the influences of the southern Indian Ocean. A striking feature that distinguishes these phases is the exchange of energy from the divergent to the rotational kinetic energy. When the monsoon becomes active, a large exchange of divergent kinetic energy to the rotational kinetic energy (strengthening the monsoon) is noted and the converse is seen during the break and the

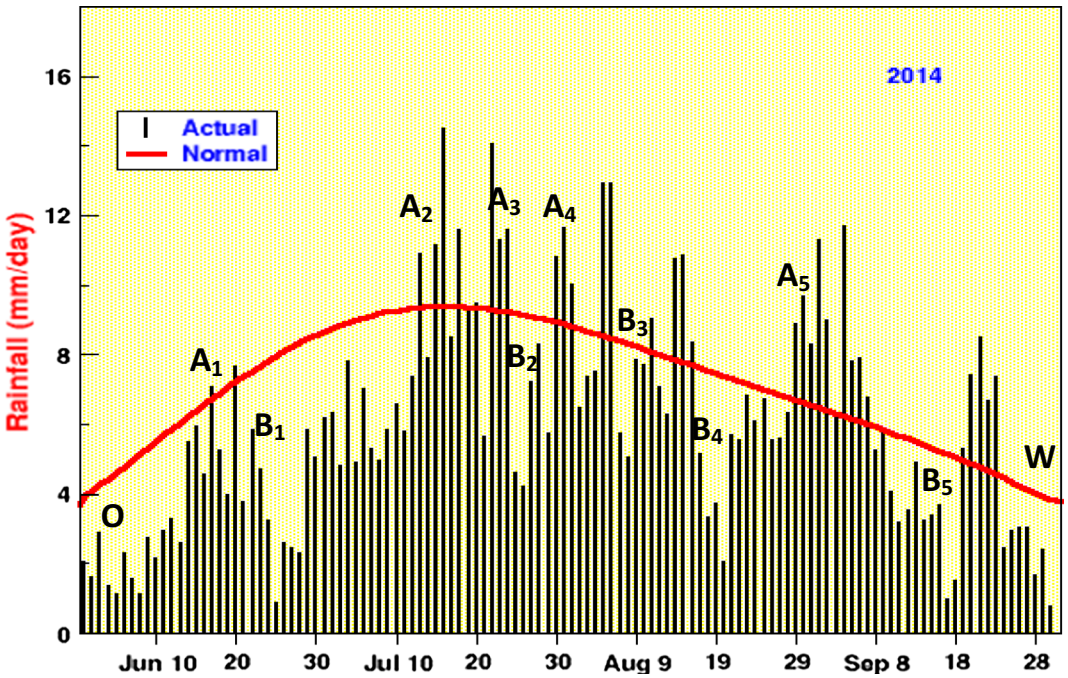

Figure 1. Evolution of all-India daily area-weighted mean rainfall (mm/day) during the monsoon 2014. The onset (O), active (A), break (B), and withdrawal (W) phases are chosen based on the daily rainfall time series.

withdrawal phases. Mapping of those features during the transitions are included here. Other aspects of the transitions include, precipitation, soil moisture, vertically integrated moisture transport vectors and the related convergence of flux of moisture, the vertically integrated heat content (moist static energy) anomalies and the vertically integrated cloud liquid water, as inferred from satellite datasets, all of these features show striking contrast among the intra-seasonal phases of the summer monsoon. These are all local features mapped over South Asia. Although these are illustrative of local contrasts, the mechanisms of the phases require us to examine outside of the south Asia domain that is addressed in part 2 of this study.

2. Data and methodology

To analyze the variations of the physical and thermodynamic variables during the intra-seasonal monsoon phase transitions, we have utilized the satellite remote sensing observations, reanalysis datasets, as well as numerical model simulations. The satellite remote sensing observations from Tropical Rainfall Measuring Mission (TRMM), Global Precipitation Measurement (GPM), and CloudSat are used to analyze the spatial and vertical distributions of the precipitation, radar reflectivity and cloud types over Indian region. The ERA Interim reanalysis datasets (Dee *et al.* 2011) from the European Centre for medium-range weather forecasts (ECMWF) are utilized to analyze the physical and thermodynamic variables described in section 4. The Indian summer monsoon season 2014, was selected for this study in favour of the overlapping data availability year for both TRMM and GPM satellites inter-comparison study.

Our choice of the phases is based on common practice, i.e., pre-onset, onset, active, break, revival and withdrawal. The onset and withdrawal phases are derived from the India Meteorological Department (IMD) criteria for onset and withdrawal, while the active and break spells were identified based on Rajeevan *et al.* (2010). These are best seen in the histograms of daily rains prepared from the all India summer monsoon rainfall datasets, such as those used in the present study. In this study for Indian summer monsoon 2014 season, the onset (6–10 June 2014), active, break and withdrawal (24–29 September 2014) phases are chosen based on the daily rains prepared from the all India summer monsoon rainfall data. Here, four active and four break spells have been selected from entire monsoon season of 2014 as shown in figure 1. The active and break spells are illustrated in figure 1 with $A_{i\ (i=1,\ldots,5)}$ and $B_{i\ (i=1,\ldots,5)}$ symbols respectively for the clarity. The active and break

spells identified were derived from TRMM and GPM daily rainfall data, based on Rajeevan *et al.* (2010). The composite of the four spells of active and break phases has been estimated to analyze the intra-seasonal phase transitions. The composite analysis has been performed for all of the physical and thermodynamic variables except the variables derived from the satellite swath datasets. The satellite swath datasets are extracted from the scanning followed by the satellite orbital path, which does not have an overlapping geo-location over Indian region for the above-mentioned all four spells of active and break phases. The intra-seasonal phase transitions of the vertical structure of rain rate are examined from TRMM precipitation radar data (TRMM 2A25). Similarly, the vertical profiles of radar reflectivity (2B-GEOPROF) and cloud types (2B-CLDCLASS) are analyzed from CloudSat data. It has been selected specific active and break spells for the intra-seasonal phase transitions analyses of TRMM 2A25, 2B-GEOPROF, and 2B-CLDCLASS datasets. A version of the WRFV3.7.1 model is used in this study to carry out the simulation to analyze the vertical structures of the hydrometeors during the monsoon phase transitions.

2.1 *TRMM/GPM datasets*

The precipitation radar was built by the Japan Aerospace Exploration Agency (JAXA) as part of its contribution to the joint US/Japan Tropical Rainfall Measuring Mission (TRMM) (Nakagawa *et al.* 2011). TRMM and GPM datasets are the most representative of the spatial distributions of rainfall and vertical structures of rain elements, over tropical region (Simpson *et al.* 1996; Huffman *et al.* 2007, 2010; Neeck *et al.* 2014; Huffman *et al.* 2015a, b). These datasets (TRMM and GPM) are used in this paper to analyze the spatial distributions of rainfall and vertical structures of clouds, during the monsoon phases of summer monsoon season 2014. The geographical distributions of rainfall are derived from the TRMM 3B42 datasets (figure 2a–d), provided at a horizontal resolution of 25 km at time interval of 3 h (Simpson *et al.* 1996). The GPM rainfall maps are derived from the Integrated Multi-satellitE Retrievals for GPM (IMERG) (figure 2e–h), those are available at a horizontal resolution of 10 km at half hourly time intervals (Huffman *et al.* 2015a, b). The vertical distributions of rain rate are derived from TRMM-2A25 datasets as shown in figure 3(a–d). The TRMM precipitation radar has a horizontal resolution at the ground of about 3.1 miles (5 km) and a swath width of 154 miles (247 km). One of its most important features is its ability to provide vertical profiles of the rain and snow from the surface up to a height of about 12 miles (20 km). The Precipitation Radar is able to detect fairly light rain rates down to about 0.027 inches (0.7 mm) per hour. At intense rain rates, where the attenuation effects can be strong, new methods of data processing have been developed that help to correct this effect. The Precipitation Radar is able to separate out rain echoes for vertical sample sizes of about 820 feet (250 m) when looking straight down. It carries out all these measurements while using only 224 watts of electric power—the power of just a few household light bulbs.

During onset (early June) of the monsoon season, most of the precipitations are observed over southern Arabian Sea, off the Kerala coast, and slowly triggers towards the Indian landmass (figure 2a and e). In mid-July, the monsoon trade winds fully covered the whole Indian landmass and having heavy spells of precipitation over central India during active phases of monsoon as shown in figure 2(b and f). The dry spell of the monsoon following the active phases is called the break phase. During the break phase, central India region receives the least precipitation as shown in figure 2(c and g). The northern India starts withdrawing the southwest monsoon trade winds early September and slowly it is withdrawing from the central India and southern peninsula (figure 2d and h). There is almost no precipitation over northern and central India during withdrawal phase. The significant variations between TRMM and IMERG estimated precipitation over both landmass and ocean are very straight forward because of the sensors used in both the datasets are different from each other, also TRMM has lesser number of sensors than IMERG (Liu 2015). However, the algorithms used to derive the precipitation for both the datasets are different from each other. IMERG precipitation datasets include the zenith angle-correction and, inter-calibrated IR fields merged from several geostationary satellites (Janowiak *et al.* 2001). Figure 3(a–d) depicts the vertical structure of rain hydrometeors from TRMM satellite. The TRMM 2A25 data are chosen from archives for the selected days closest to each of the transitioning phases of monsoon 2014 season and are analyzed here. Figure 3(a) shows

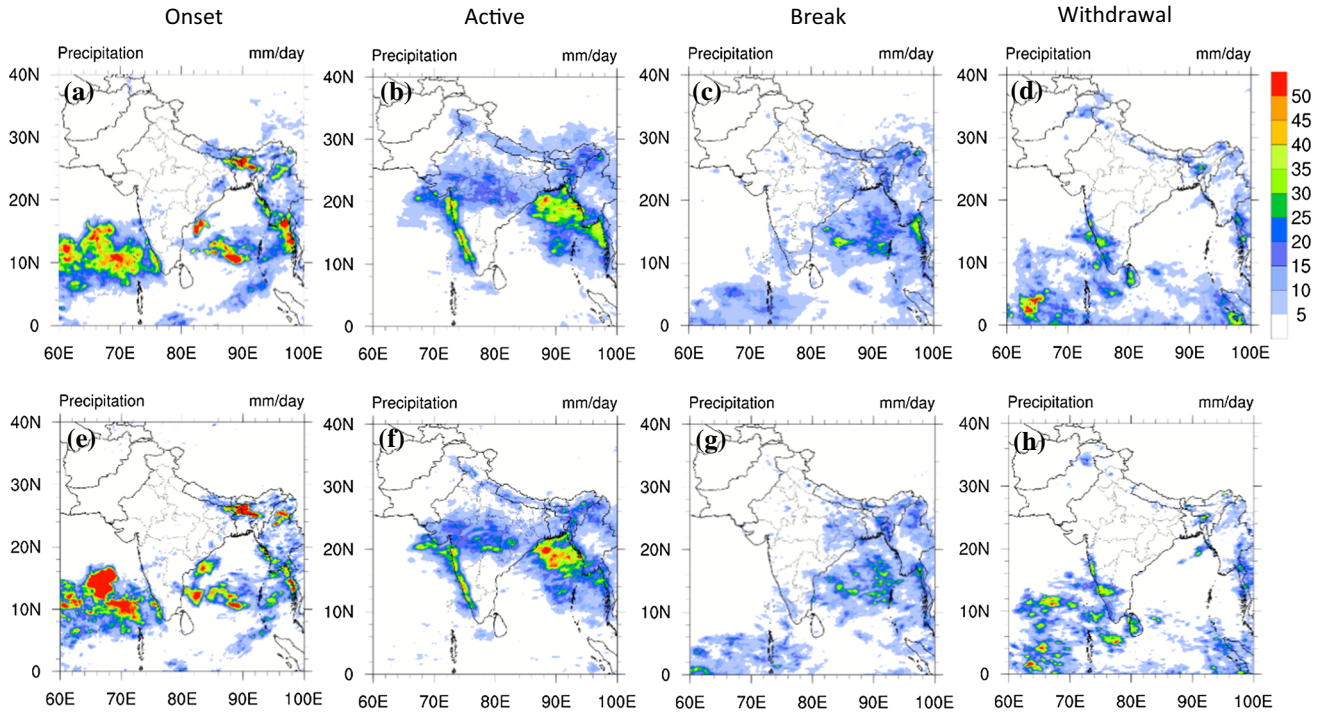

Figure 2. The TRMM (**a–d**) and GPM/IMERG (**e–h**) derived rainfall (mm/day), for onset, active (composite), break (composite) and withdrawal phases for monsoon 2014.

deep overshooting cumulonimbus reaching almost 6–7 km during the onset phase. During active phase, the nimbostratus and cumulonimbus are dominant (figure 3b). During break phase, weak nimbostratus clouds are still present (figure 3c). Figure 3(d) shows the rainfall during withdrawal phase.

2.2 *CloudSat datasets*

The Cloud Profiling Radar (CPR) onboard the CloudSat (Stephens *et al.* 2002) is a 94-GHz nadir-looking radar which measures the power backscattered by clouds as a function of distance from the radar. The CloudSat CPR operating at 94-GHz ($\sim$3 mm) measures the backscattered power from the cloud- and precipitation-size particles. The CPR resolution is 1.5 km cross-track by 2.5 km along-track of radar footprint. The CPR pulse width is $\sim$3.3 µs and thus has a vertical resolution of $\sim$480 m. The CPR data oversamples at $\sim$240 m. Details about the CloudSat measurements are given in http://cloudsat.atmos.colostate.edu. Figures 4 and 5 depict the vertical distributions of rain hydrometeors and cloud classifications from 2B-GEOPROF and 2B-CLDCLASS products respectively, derived from the CloudSat satellite measurements. A radar reflectivity (dbz) factor from the CloudSat, 2B-GEOPROF data is shown in figure 4(a–d) for the onset, active, break and withdrawal phases respectively. The satellite pass locations are shown in the inset diagram (top left corner of each panel). Figure 4(a) shows a narrow vertically stretched intense radar reflectivity during this onset period at around 12°N latitude. During the active phase in July a much wider latitudinal band of intense convection is shown by the radar reflectivity that stretches between 16° and 25°N latitudes. The height of radar reflectivity is confined below the 13-km level during active phase, whereas during the onset phase the reflectivity suggested rather deep clouds stretched up to 16 km. These features are absent during the break and the withdrawal phases.

CloudSat also provides an inventory product 2B-CLDCLASS, which classifies cloud types. Those datasets for the same satellite pass as of 2B-GEOPROF are shown in figure 5(a–d). The segments of the satellite path, which lie over the Indian landmass are chosen from its orbital track. The segment-17 (latitude 5.5–17.1°N) and segment-18 (latitude 17.1–28.6°N) mostly cover the active monsoon regions of Indian landmass from south to north. Segment-17 is chosen for the onset cloud classification, since during the onset period the monsoon clouds are mostly covered the regions below 20°N of the Indian landmass. During end of June and early July, monsoon clouds mostly cover the central and northern India, which help to

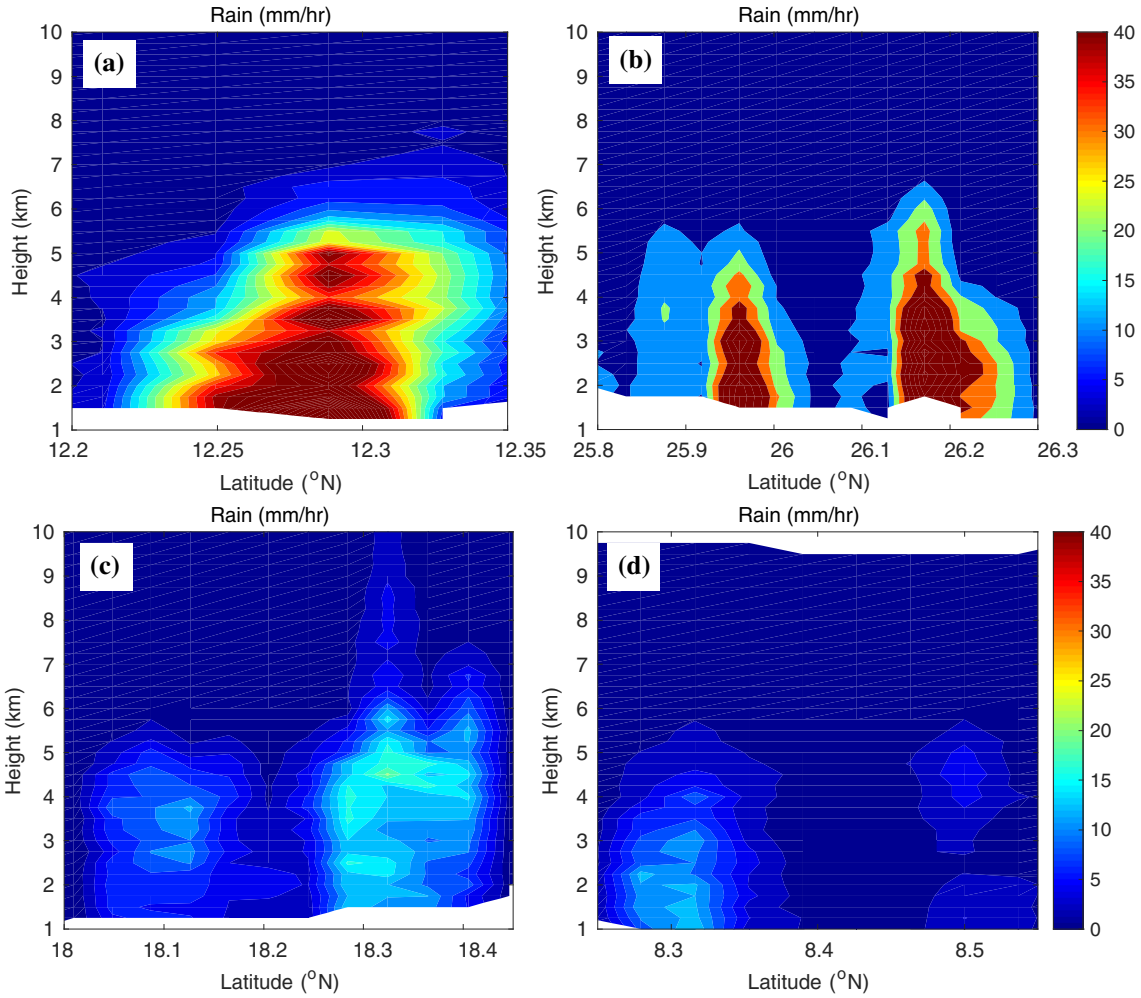

Figure 3. Vertical structure of rain rate (mm/h) from TRMM 2A25 PR datasets for selected satellite pass during (**a**) onset (06 June 2014), (**b**) active (22 July 2014), (**c**) break (17 August 2014) and (**d**) withdrawal (24 September 2014) phases of monsoon 2014.

choose segment-18 for rest of the monsoon phases. The onset phase is characterized by deep cumulonimbus clouds; to the north and south of this region, the satellite pass shows a wide stretch of Alto stratus clouds. During the active phase, a predominant stretch of cumulonimbus clouds is noted over most of India. A near total absence of such deep cloud, along the satellite pass, are noted during the break and withdrawal phases.

2.3 *ERA-interim datasets*

Datasets like wind fields, moisture flux, geopotential height, temperature and specific humidity used in this study are obtained from ECMWF's ERA-Interim reanalysis (Dee *et al.* 2011). ERA-Interim project was initiated to provide a better quality reanalysis product by improving on certain key aspects of ERA-40, such as representation of the hydrological cycle, quality of the stratospheric circulation, and handling biases and new observing systems. ERA-Interim reanalysis datasets have relatively good horizontal, vertical and temporal resolutions as compared to other available reanalysis datasets. The system includes a 4-dimensional variational analysis (4D-Var) with a 12-h analysis window. The spatial resolution of the dataset is approximately 80 km (T255 spectral) on 60 vertical levels from the surface up to 0.1 hPa. Daily, a million of observational datasets acquired from various sources, e.g., aircraft, balloons, satellite, and ground stations are assimilated to create reanalysis ERA-Interim datasets.

3. Cloud resolving model (WRF)

A version of the WRFV3.7.1 model carrying the following physics/microphysics options was used to examine the vertical structure of clouds covering the different phases of the monsoon during the summer

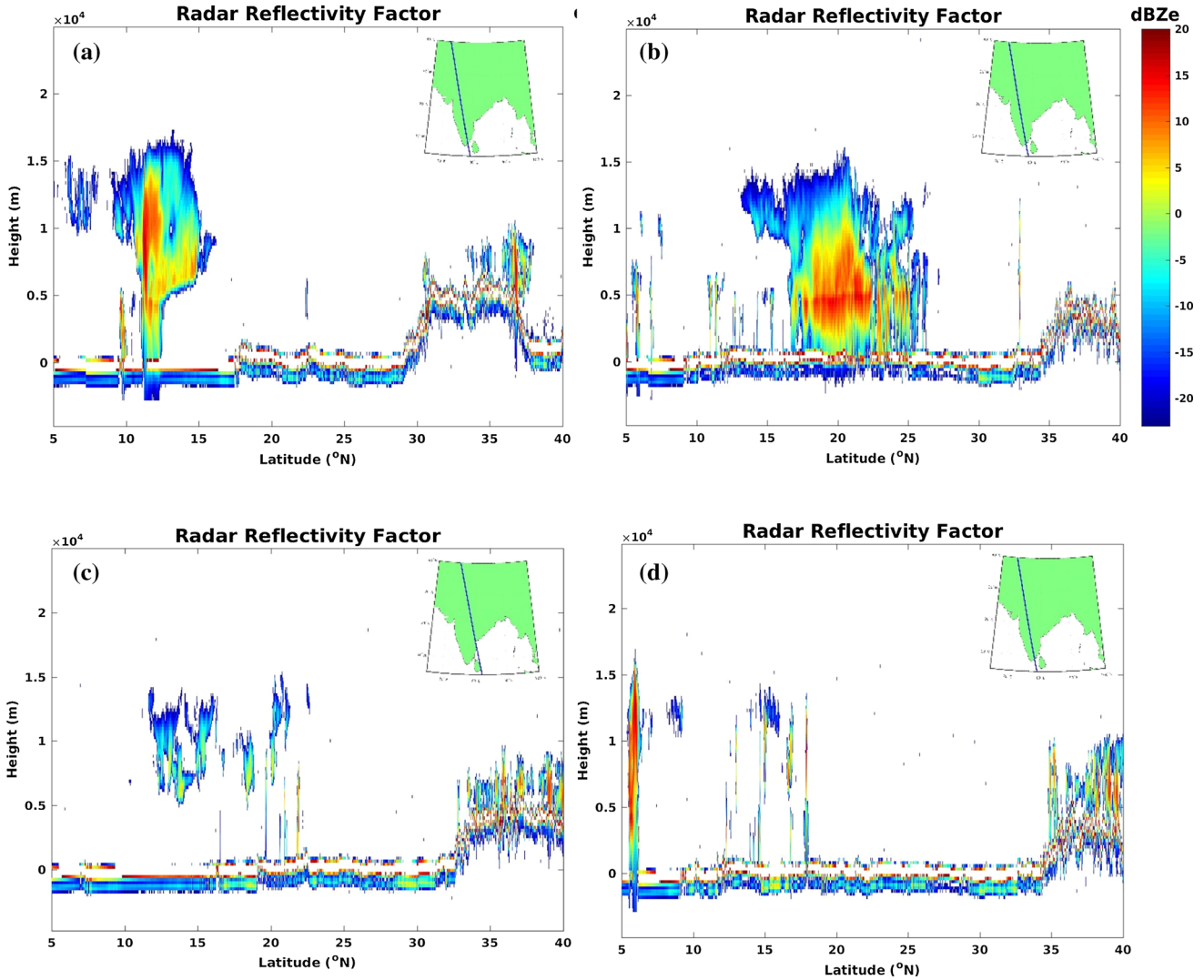

Figure 4. The 2B-GEOPROF radar reflectivity (dbz) from CLOUDSAT satellite measurement along the satellite track passes over Indian landmass (inset) during the (**a**) onset (8 June 2014: Granule No.: 43153), (**b**) active (22 July 2014: Granule No. 43794), (**c**) break (18 August 2014: Granule No. 44187), and (**d**) withdrawal (24 September 2014: Granule No. 44726).

monsoon season of 2014. The WRF model carries three nests (1, 3 and 9 km) with 46 vertical levels. Goddard microphysics (Lin *et al.* 1983 as modified by Tao *et al.* 2009); the precipitation processes for the inner two nests that are non-hydrostatic and are - cloud resolving. The outer nest (9-km horizontal resolution) carries the Kain–Fritsch cumulus parameterization scheme (Kain and Fritsch 1993). The long wave radiative transfer utilizes the rapid radiative transfer scheme based on Mlawer *et al.* (1997). The short wave radiative transfer utilizes the scheme proposed in Dudhia (1989). The cloud specifications for radiative transfer are based on the diagnostic clouds that are threshold relative humidity dependent. The planetary boundary layer in this model is based on the Yonsei University's PBL scheme (Hong *et al.* 2006). Initial conditions for the model are derived from the GFS (Global Forecast System) analysis which upon space time interpolation, provides time-dependent lateral boundary conditions following the time steps of the WRF model. This was the same version of the model that was recently used for studies of extreme rains over India (Krishnamurti *et al.* 2016). For the model output parameters, we followed a recent study by Tao *et al.* (2016) to extract vertical structures of cloud and hydrometeors. Several model runs were made during each phase of the monsoon transitions.

3.1 *Vertical structures of hydrometeors from cloud resolving model*

The cloud resolving model, described in section 3 was used to make many 2-day long experiments during each phase of the Indian summer monsoon 2014 to extract the vertical structure of model

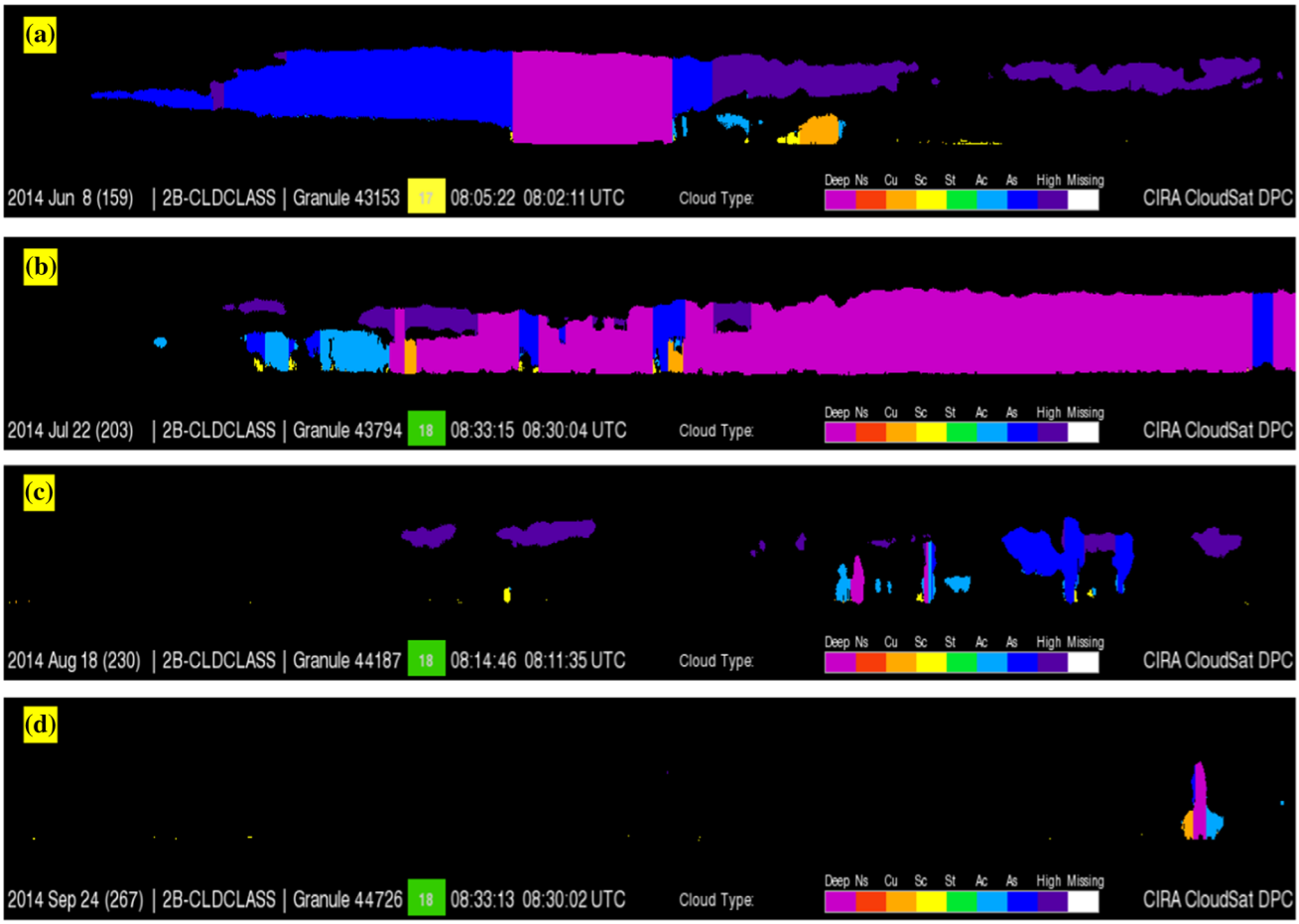

Figure 5. The cloud classifications from 2B-CLDCLASS data product from CLOUDSAT satellite measurements during the (**a**) onset (8 June 2014: Granule No.: 43153), (**b**) active (22 July 2014: Granule No. 43794), (**c**) break (18 August 2014: Granule No. 44187), and (**d**) withdrawal (24 September 2014: Granule No. 44726). The segments are selected from the corresponding satellite orbital tracks as shown in figure 4 for 2B-GEOPROF radar reflectivity. The segment-18 (Lat: 17.1–28.6) and segment-17 (Lat: 5.5–17.1) are chosen based on their geographical pass over Indian landmass.

implied radar reflectivity and the vertical profiles of hydrometeors such as snow, ice, rain, graupel and cloud. In this presentation, we followed the study of Tao *et al.* (2016). Such experiments were also carried out for other years to confirm the representative nature of the results of the 2014 season. Figure 6(a–d) shows the model-based radar reflectivity for the onset, active, break and withdrawal phases of monsoon 2014. It shows the vertically tall cumulonimbus-like structures (extending vertically to almost 16 km) during the onset phase and more of altostratus/nimbostratus type structures (extending up to 10 km) during the active phase. As expected, the vertically extended clouds are not seen during the break and withdrawal periods.

The vertical structure of hydrometeors can be examined using a microphysical cloud resolving model following Tao *et al.* (2016). The WRF model is used to examine the vertical structures of rain, snow, cloud, ice and graupel over central India (20–27.5°N and 75–82.5°E) during the transition phases of the monsoon. Figure 7(a–d) shows these respective results for the onset, active, break and withdrawal phases. The units along the abscissa for all graphs are in kg/kg. It must be noted that the scale along the abscissa is not the same in all panels of figure 7. The largest magnitudes are seen for the active (composite) phase (figure 7b) where the numbers are multiplied by 10^{-4}, whereas the other panels are smaller, and the multiplication factor is 10^{-5}. The vertical scale in all panels are height in kilometers. What stands out in these illustrations is the active phase, when the rain below 10 km has robust values of the order of 2.0×10^{-4} (figure 7b). Ice and graupel carry their importance above the 9-km level from the anvils of the upper troposphere during the active phase and the other phases over central India. The graupel is also large during the onset phase (figure 7a), but in an order of

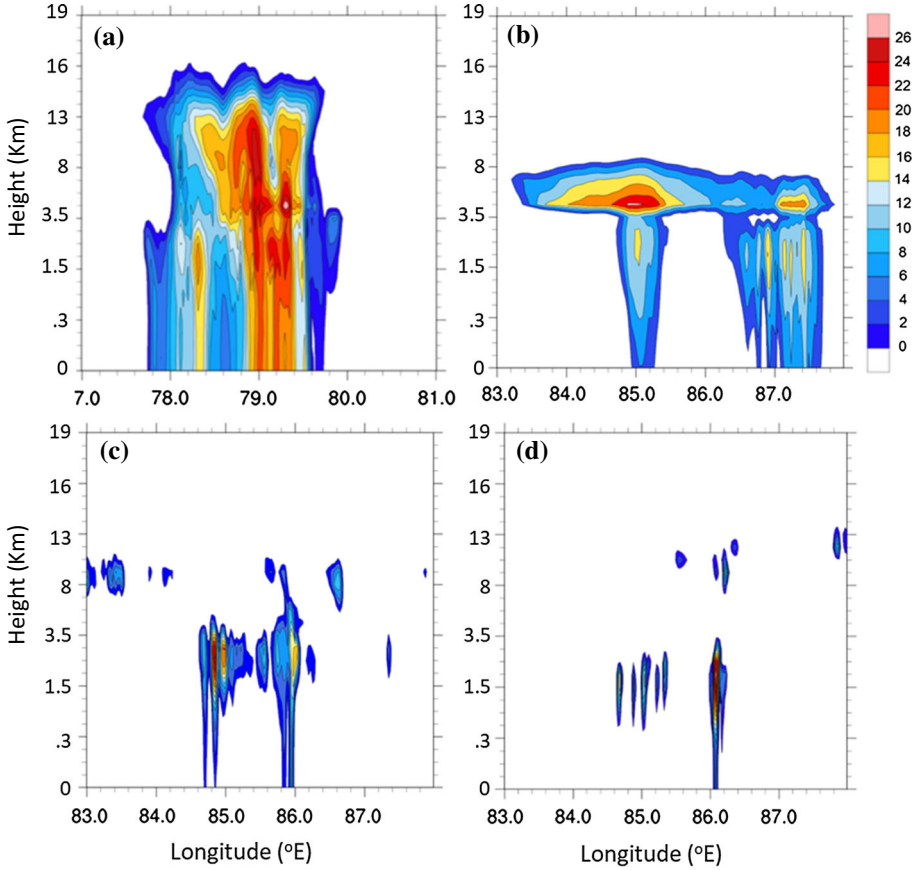

Figure 6. The profiles of vertical structures of radar reflectivity (dBZ) derived from cloud resolving model (WRF) simulation during (**a**) onset, (**b**) active (composite), (**c**) break (composite) and (**d**) withdrawal phases of monsoon 2014.

magnitude smaller than the active phase (figure 7b). The break (composite) phase does show some rains but is not robust in any other class of hydrometeors (figure 7c). The withdrawal phase in general has much smaller values. The other model simulated variables, such as wind and rainfall are coherent with reanalysis dataset. It may be noted that, we have shown only few figures from model simulation in this manuscript.

4. Monsoon phase transitions in various parameters

4.1 *Wind streamlines at 850 hPa level*

The flow field at 850 hPa level shows rather striking contrasts among the onset, composite active, composite break and withdrawal phases during the 2014 season derived from ERA-Interim datasets. The respective streamlines of the 850 hPa level flow field are shown in figure 8(a–d). The onset phase (figure 8a) shows an onset vortex over the Arabian Sea (Krishnamurti *et al.* 1981), and this feature shows up during onset in 2 out of 3 years. The westerlies to the south of the vortex bring in moist winds and the onset of monsoon rains over Kerala; to the north of the vortex northwesterly dry air prevails during this period. The active phase shown here carries strong (moist) monsoon westerlies south of 20°N from the Arabian Sea (figure 8b). This period was also characterized by a monsoon depression over the eastern part of India. That feature brought in rains and moist air from the Bay of Bengal. These circulation features are rather typical of the active phase of the monsoon. The break phase shows weaker westerlies over most of India with a small northerly wind component over most places (figure 8c). The withdrawal phase carries some very striking features such as the stronger northerly wind components over most of India (figure 8d). During this late September period, the rainfall activity moves south from the eastern foothills of the Himalayas towards Myanmar. Almost every year these daily map features during the phases of monsoon show similar transitions.

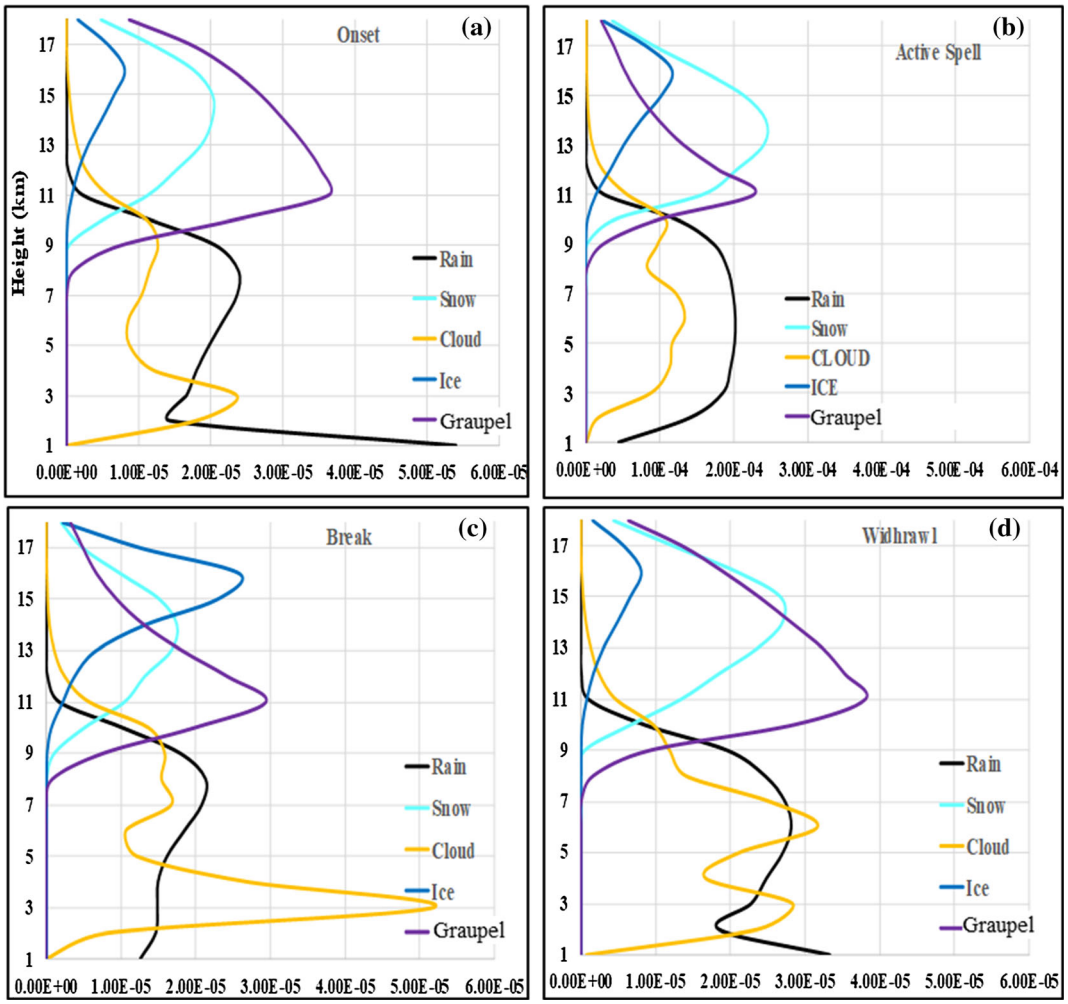

Figure 7. The profiles of the vertical distributions of domain averaged (Central India: 20–27.5°N and 75–82.5°E) rain, snow, cloud, ice and graupel derived from cloud resolving model (WRF) simulations during (**a**) onset, (**b**) active (composite), (**c**) break (composite) and (**d**) withdrawal phases of summer monsoon 2014. The abscissas show mixing ratio with units kg/kg.

4.2 *The ISO fields at 850 hPa level*

The ISO which describes the intra-seasonal oscillations during a season are one of the most robust features of the monsoon. This can be mapped rather easily using a band passed filter, of the wind field, to extract the ISO time scale winds, that reside in the same time scale as the MJO, i.e., 30–60 days (Krishnamurti and Subrahmanyam 1982). Those fields at the 850 hPa level show the clear northward passage of these waves, alternating between cyclonic and anticyclonic lobes. The rate of meridional propagation is around one-degree latitude per day and the meridional wave length is around 3000 km. Figure 9(a–d) illustrates the ISO wind field of onset, composite active, composite break and the withdrawal phases respectively during the monsoon season 2014 derived from ERA-Interim datasets. The onset period (figure 9a) during June sees two major cyclonic lobes providing southwesterly flows into southern India, these winds carry an amplitude of 1–3 m/s and that contributes to an enhancement of the monsoon circulation. These are called a parallel mode during the onset when the ISO and the climatology both enhance the south-westerly monsoon circulation over south-east India. In contrast, during the break phase (figure 9c) the ISO time scale winds are anti-parallel to the climatology and they weaken the monsoon. During the active phase (figure 9b), the cyclonic lobes (that were seen during the onset) have moved farther north and provide a parallel mode for the climatology and enhance the south-westerly flow over most of southern India where moisture from the Arabian Sea contribute to the rains of the active period. During this same active phase, the flows north of the cyclonic lobes of the ISO bring in moisture from the Bay of Bengal that contribute to heavy rains

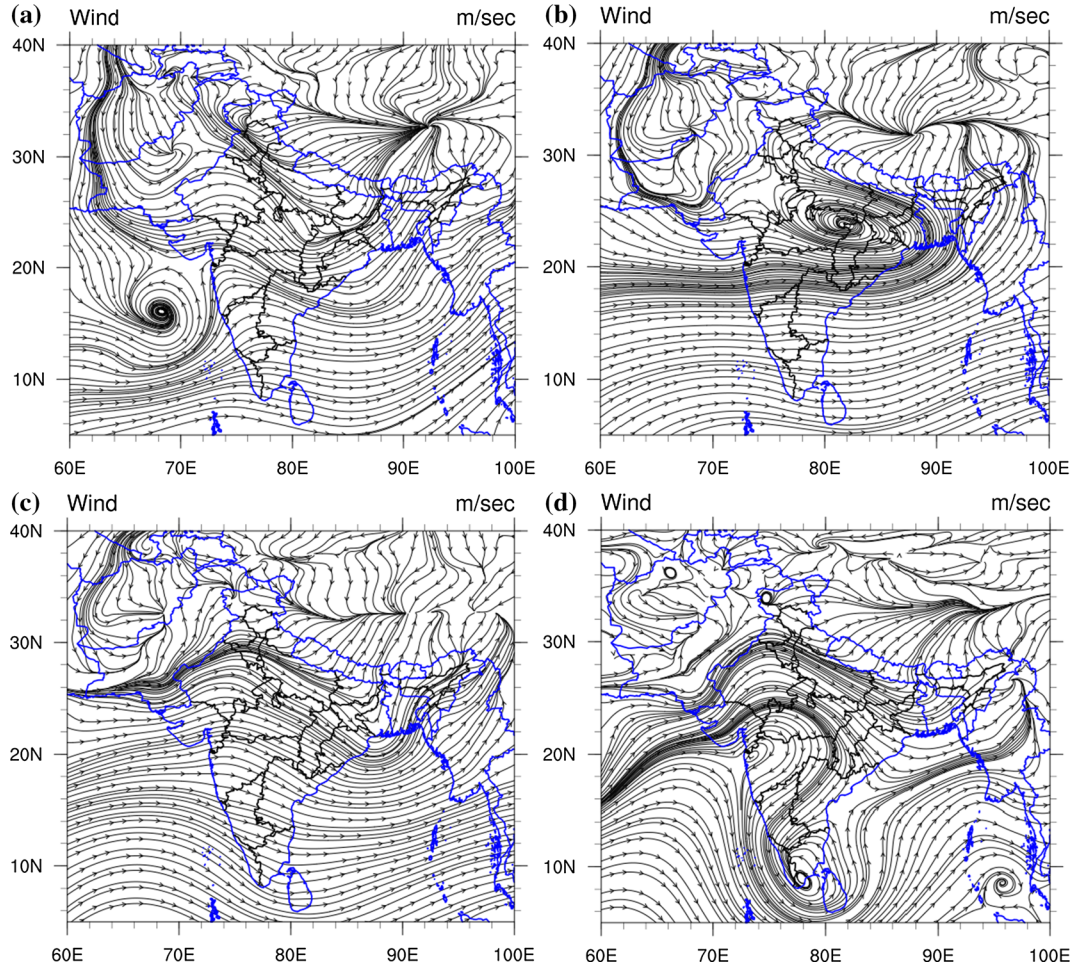

Figure 8. Spatial patterns of the wind streamlines at 850 hPa over Indian region during (**a**) onset, (**b**) active (composite), (**c**) break (composite), and (**d**) withdrawal phases of monsoon 2014 derived from ERA-Interim datasets.

over central and northern India. The direction of the winds of the ISO during the withdrawal phase (figure 9d) are essentially opposite to that of the active phase and these contribute to a weakening of the summer monsoon.

4.3 *Surface energy balance*

Figure 10(a–d) shows the model-based computation of the variations in the surface energy balance during the transitions of phases of the life cycle of Indian summer monsoon season of 2014. Here in figure 10, DL_Rad, UL_Rad, US_Rad, LH_Flx, SH_Flx and DS_Rad represent Downward Longwave Radiation, Upward Longwave Radiation, Upward Shortwave Radiation, Latent Heat Flux, Sensible Heat Flux and Downward Shortwave Radiation, respectively. The vertical bars in this illustration show the upward and downward directed short- and long-wave radiation reaching the earth's surface over central India, enclosed between 20 and 27.5°N latitudes and 75–82.5°E longitudes. It also includes bars for the surface fluxes of latent and sensible heat. The onset, composite active, composite break and withdrawal phases are illustrated here (figure 10a–d). The downward directed shortwave radiation during onset, active, break and withdrawal phases are 325, 230, 310 and 280 W/m^2, respectively. The larger values during the onset and the break phases are clearly due to the much lower cloud cover compared to the active and the withdrawal phases. The reflected short-wave radiation for these respective phases are 81, 57, 78, and 72 W/m^2 based on a surface albedo over central India of close to 0.4. The upward long-wave radiation, depends on the surface temperatures, these respective surface fluxes are 540, 430, 490, and 460 W/m^2. The warmest surface temperatures over central India are a carryover from the pre-onset surface heating. The downward directed long-wave radiation at the earth's surface carried the values during the

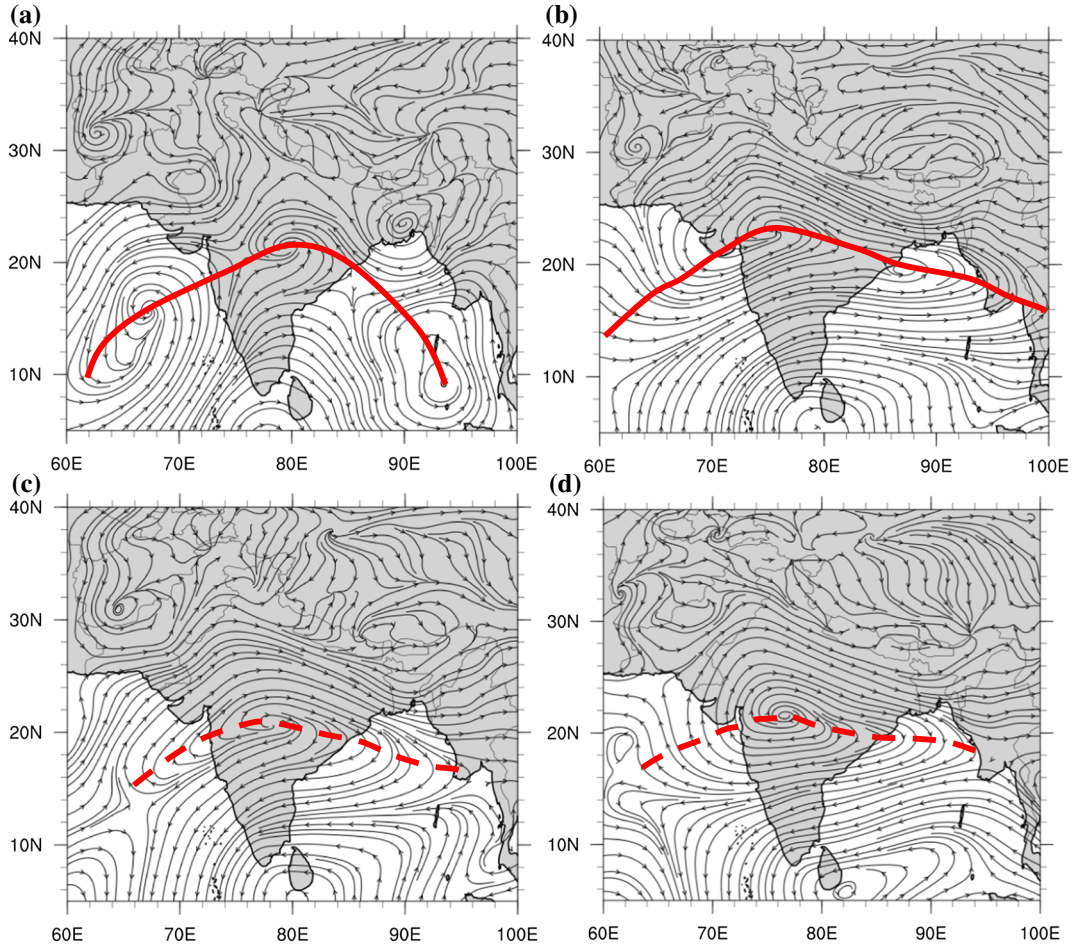

Figure 9. Streamline isotachs at 850 hPa from Butterworth low pass filter (30–60 days) estimated from ERA Interim datasets during (**a**) onset, (**b**) active (composite), (**c**) break (composite) and (**d**) withdrawal phases of monsoon 2014 derived from ERA Interim datasets. The solid red line marked the counterclockwise circulation of monsoon axis and dashed red line marked the clockwise circulation of monsoon axis.

respective monsoon phases are 430, 440, 420, and 370 W/m^2. The active phase carries the larger values because of the warm troposphere below the Tibetan high circulations.

The upward flux of sensible heat during these respective phases are 130, 5, 120 and 15 W/m^2. During the active phase the surface maximum temperatures in raining regions go down to values as low as 26 °C as compared to the onset phase, when many parts of the domain still carry surface temperatures as high as 40 °C. The low values of the withdrawal phase relate to the location of the overhead Sun in September when that is close to the equator. The upward flux of latent heat is a strong function of soil moisture, those respective values are 25, 145, 50 and 155 W/m^2 during onset, active, break and withdrawal phases, respectively. The overall soil over the central India domain is still quite dry during the onset and latent heat fluxes are small, the large fluxes during active phase are related to the increase in soil moisture. During break phase, latent heat flux is larger than the onset phase due to the retention of soil moisture from the active phase, which carries during the break phase. The season long rains and the accumulated soil moisture accounts for large latent heat fluxes as the withdrawal continues. Overall cloud cover and soil moisture are most important factors for the transitions in the surface energy fluxes during these respective phases.

4.4 *Soil moisture*

The geographical distribution of soil moisture anomaly is estimated from the ERA-Interim reanalysis (Dee *et al.* 2011) during the monsoon phase transitions for the onset, composite active, composite break and the withdrawal phases are shown in figure 11(a–d), respectively. These illustrations show large changes in soil moisture during

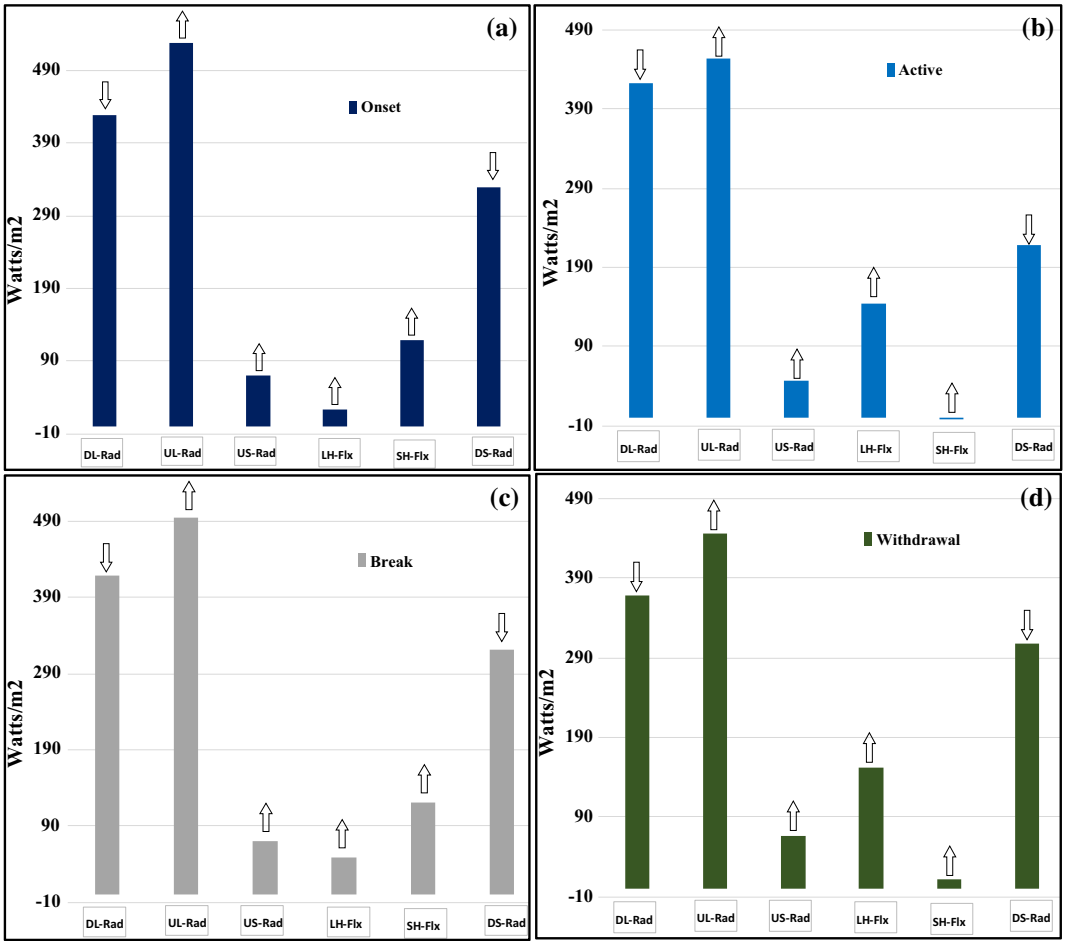

Figure 10. Surface energy balance during the (**a**) onset, (**b**) active (composite), (**c**) break (composite) and (**d**) withdrawal phases of monsoon 2014 derived from the cloud resolving model (WRF) simulation. All the variables are domain averaged over central India (20–27.5°N and 75–82.5°E). Here DL_Rad, UL_Rad, US_Rad, LH_Flx, SH_Flx and DS_Rad represent Downward Longwave Radiation, Upward Longwave Radiation, Upward Shortwave Radiation, Latent Heat Flux, Sensible Heat Flux and Downward Shortwave Radiation respectively.

these phase transitions. The lowest values of the soil moisture at the onset phase (figure 11a) are clearly related to months of dry spring season prior to the onset. The soil moisture increases as the onset occurs and continues to increase drastically during the successive active phases (figure 11b). The first break phase comes too soon after the first short active spell and sees quite low values of soil moisture (not shown here). By the second break phase, the soil moisture decreases some, but due to the retention of water in the soil for periods of a week (Bounoua and Krishnamurti 1993), the soil moisture does not revert to the onset or to the first break phase values (figure 11c). During the withdrawal phase (figure 11d) of mid-September, the retention of the soil moisture from season long rains, continues to hold large values compared to the onset or even the first break period values. The larger values of soil moisture during the second break usually helps the next revival phase (not shown here), where the revival includes some small recycling of surface water, most of the moisture supply to account for the revival rains however comes from lateral eddy flux convergence of moisture.

4.5 *Moisture flux*

The vertically integrated moisture transport vectors and convergence of flux of moisture transport over south Asia show major differences in the geographical distributions during the monsoon phase transitions. The detailed formulation of moisture transport is given in "Appendix". The moisture fluxes across the west coast of India undergo large variations in relation with active/break cycle of the monsoon (Cadet and Greco 1987a, b). The following illustration for the onset,

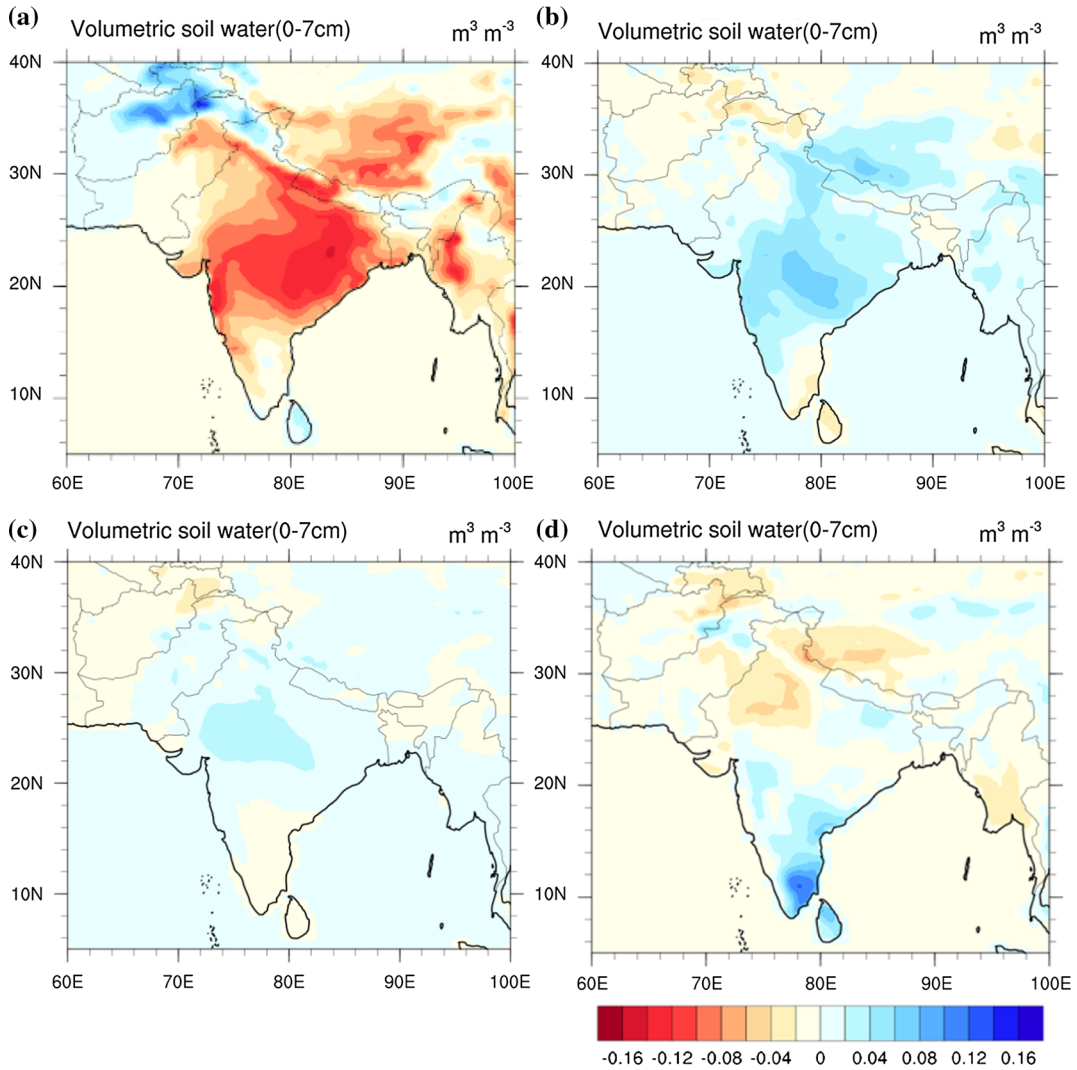

Figure 11. Spatial distribution of anomaly of soil moisture during (**a**) onset, (**b**) active (composite), (**c**) break (composite) and (**d**) withdrawal phases of monsoon 2014 derived from ERA Interim datasets.

active, break, and the withdrawal phases of the 2014 monsoon season are shown in figure 12(a–d).

During the onset phase, the moisture transport vectors are from south-westerly and westerly direction over the Arabian Sea facing the Kerala coast with some maxima in the moisture convergence belt with values as high as 2×10^{-4} kg m^{-1} s^{-1} (figure 12a). Similar moisture transport vectors from the south-westerlies are also prevalent over the Bay of Bengal. Those are related to the Myanmar monsoon's moisture belt. During active phases, there are strong westerlies all over Arabian Sea from south to north and an anticlockwise circulation over central and eastern India, carrying much higher moisture convergence ($>4 \times 10^{-4}$ kg m^{-1} s^{-1}) over central and eastern India (figure 12b). Similar pattern of westerly moisture fluxes is seen all over the Indian landmass and Bay of Bengal. Also, there are higher moisture convergence ($>2 \times 10^{-4}$ kg m^{-1} s^{-1}) over Bay of Bengal and north-eastern India as compared to onset, break and withdrawal phases. This active phase during 2014 was anomalous, in that rainfall was deficient over some parts of Indo-Gangetic plains and West Bengal. During the break phases, there are westerly moisture fluxes over south of Kerala coast, however, the westerlies are much weaker over northern Arabian Sea and Gujarat coast, as compared to active and onset phases (figure 12c). Much lesser moisture convergences ($<1 \times 10^{-4}$ kg m^{-1} s^{-1}) are also noted over Western Ghats area during the break phase. Westerlies are also prevailed over Bay of Bengal, however with lesser moisture convergences ($<1 \times 10^{-4}$ kg m^{-1} s^{-1}) as compared to active phase. During withdrawal, there are northeasterly moisture fluxes present over southern part of India, and an anticyclonic circulation prevailed over

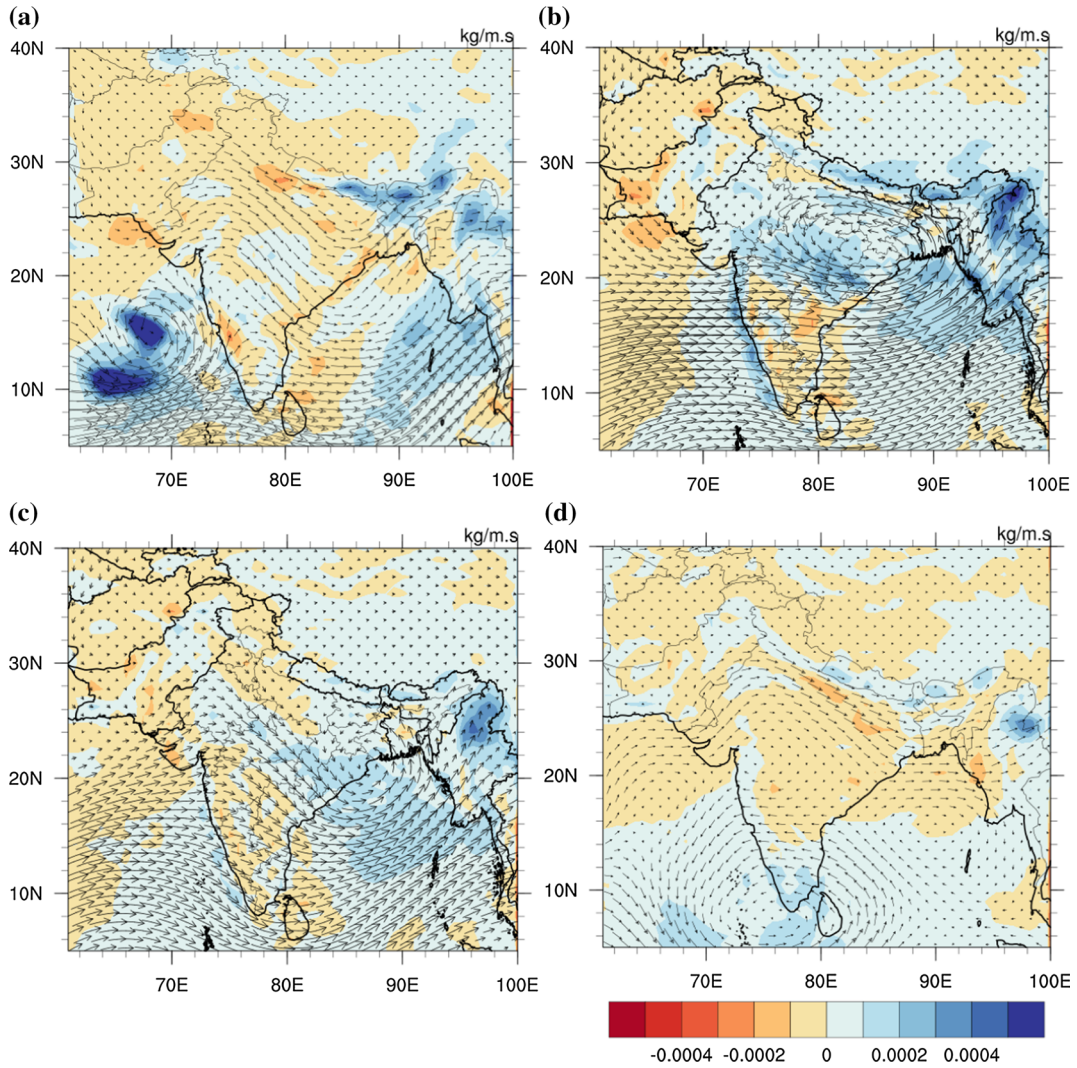

Figure 12. Spatial distribution of vertically integrated moisture flux (vector) and moisture convergence/divergence [+ve/–ve (kg m^{-1} s^{-1}): shaded] derived from ERA Interim datasets during (**a**) onset, (**b**) active (composite), (**c**) break (composite) and (**d**) withdrawal phases of monsoon 2014.

southern peninsular India (figure 12d). The moisture convergences over the Western Ghats are now lower in magnitude ($<1 \times 10^{-4}$ kg m^{-1} s^{-1}) as compared to onset, active and break phases. North-easterly moisture transport vectors prevail over the north-east India and northern Bay of Bengal.

4.6 *Moist static energy*

The vertically integrated moist static energy is a measure of the heat content. That field is extremely important for studies of monsoonal link with the extra-tropics (Krishnamurti *et al.* 2016). Figure 13 shows the anomaly of the vertically integrated moist static energy during the onset, active, break and withdrawal phases of monsoon 2014. The biggest change in this field occurs between the onset phase and the active phase of the monsoon, especially in the western foot hills of the Himalayas (figure 13a and b), where the heat content anomaly goes from the largest negative values to large positive values. This transition in the values of the anomaly of the vertically integrated $gZ + C_pT + L_q$ arise largely from the transition of a dry to a very wet atmosphere during the active phase. The product of the moist static energy and the wind is a measure of the heat transport at any point in the atmosphere in the direction of that wind. The convection of the active phase has a large amount of buoyancy that results in the generation of large potential energy (gZ), as the giant Tibetan high forms. That potential energy largely comes from a loss of sensible heating (C_pT) during the buoyant ascent of parcels. A local moist adiabat is a very interesting nonlinear triad, where the mutual exchanges of energy among these three components, during moist adiabatic ascent, is very

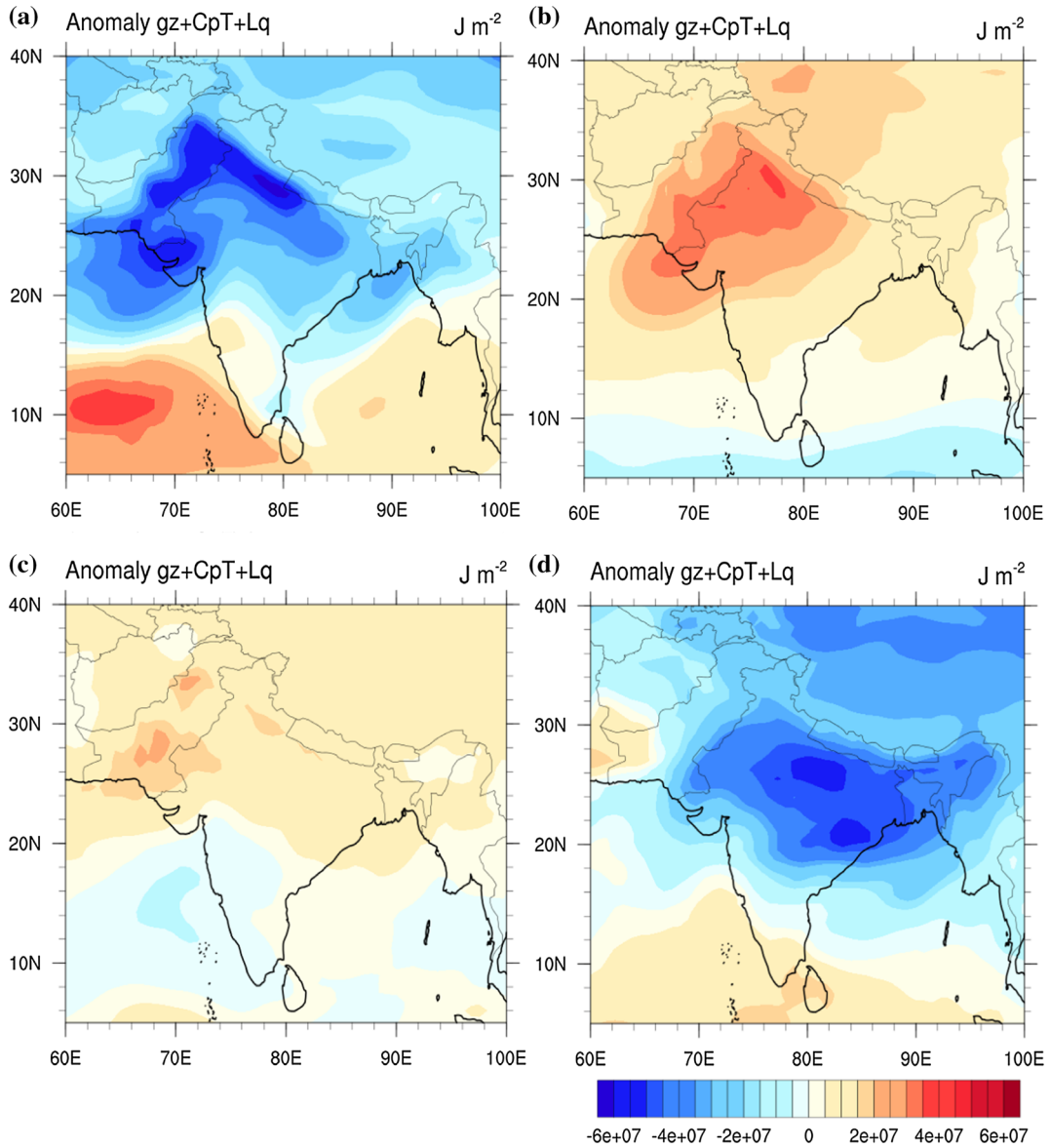

Figure 13. Spatial distribution of anomaly of vertically integrated moist static energy (gz + C_pT + Lq) derived from ERA Interim datasets during (**a**) onset, (**b**) active (composite), (**c**) break (composite) and (**d**) withdrawal phases of monsoon 2014.

revealing on the role of latent heating (L_q). Latent heating provides some energy to the sensible heating; however, it is the buoyancy provided by changes on cloud virtual temperatures that facilitates the largest exchange from sensible heating to the potential energy. Krishnamurti *et al.* (2016) have discussed the implications of large heat content anomalies during the active phase, resulting from extreme rain events. The extreme rain events lead to sudden increase of the positive values of the heat content anomaly that excite the formation of a thermodynamical wave trains which traverses around the Tibetan high to the north of the Himalayas and rides along the jet (this jet located north of the Himalayas) starts at around 30°N and moves as far north as 50°N by 120°E longitude. These features provide a major link for the monsoonal link for the recent rapid Arctic ice melt. The intensity of the monsoon of the active phase is important for such extratropical links (Krishnamurti *et al.* 2016). The break phase and especially the withdrawal phase of the monsoon do not show any such large positive heat content anomalies.

4.7 *Exchange from the divergent to the rotational kinetic energy (ψ–χ interactions)*

The salient terms for the energy exchange from the divergent kinetic energy into rotational kinetic energy are expressed by $\overline{\overline{f\nabla\psi\cdot\nabla\chi}}$ and $\overline{\overline{\zeta\nabla\psi\cdot\nabla\chi}}$ (where $\zeta=\nabla^2\psi$), respectively the 1st and 2nd term

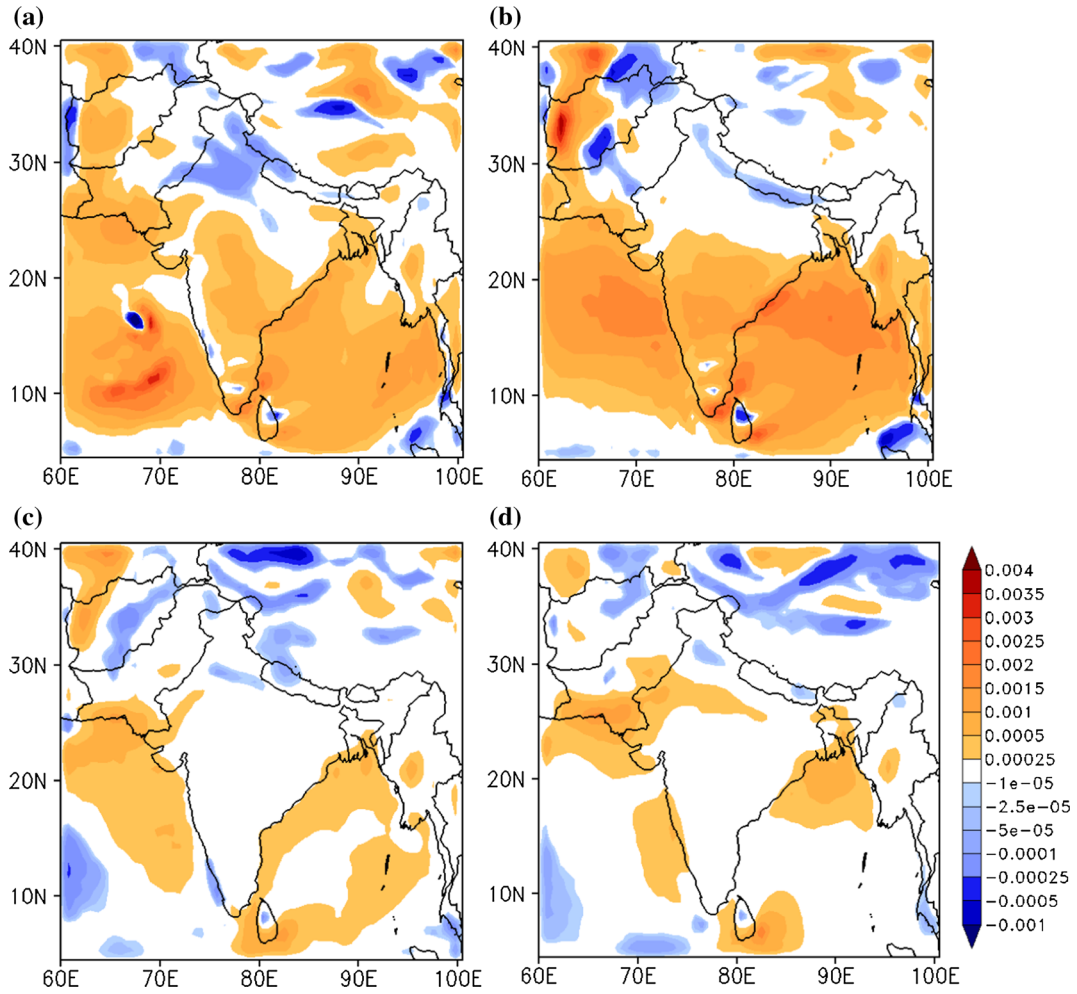

Figure 14. Spatial distributions of the sum of term 1 and term 2 ($m^2\ s^{-3}$) from $\psi-\chi$ interactions described in Eq. (1), i.e., $(f\overline{\overline{\nabla\psi\cdot\nabla\chi}}+\overline{\overline{\nabla^2\psi\nabla\psi\cdot\nabla\chi}})$ at 850 hPa during (**a**) onset, (**b**) active (composite), (**c**) break (composite), and (**d**) withdrawal phases of monsoon 2014 derived from ERA Interim datasets.

derived from the energy equation $\frac{\partial}{\partial t}K_\psi$ (Krishnamurti *et al.* 2006) and given by:

$$\frac{\partial}{\partial t}\overline{\overline{K_\psi}} = \left[\overline{\overline{f\nabla\psi\cdot\nabla\chi}}+\overline{\overline{\zeta\nabla\psi\cdot\nabla\chi}}+\overline{\nabla^2\chi\frac{(\nabla\psi)^2}{2}}+\overline{\overline{\omega J\left(\psi,\frac{\partial\chi}{\partial p}\right)}}\right]+\overline{\overline{F_\psi}} \quad (1)$$

where $\overline{\overline{()}}$ denotes integration over a three-dimensional (x, y, p) closed domain. The terms within the brackets on the right-hand side of Eq. (1) involve both ψ and χ, and provide the interaction between the rotational and divergent parts of the wind (i.e., $\psi-\chi$ interactions). The first and second terms in the bracket are the most important terms for energy exchange. The third and fourth terms were calculated and found much smaller in magnitude as compared to the first two terms, the same was noted in the Krishnamurti and Ramanathan (1982). $\nabla\psi$ and $\nabla\chi$ are important vectors in the energy exchange from the divergent to the rotational kinetic energy. These vectors measure the gradients of the stream function and the velocity potential, their mutual orientations (i.e., the angle between these two vectors) are important. If the angle is >0° and <45°, then the exchange from the divergent to the rotational kinetic energy would be large. The converse is true if the angle is >135° and <180°. The net exchange from divergent to the rotational kinetic energy also depends on the magnitude of the absolute vorticity that multiplies the dot product of these two vectors.

The sum of term 1 and term 2 $(\overline{\overline{f\nabla\psi\cdot\nabla\chi}}+\overline{\overline{\zeta\nabla\psi\cdot\nabla\chi}})$ was mapped at the 850 hPa level for the onset, active, break and withdrawal phases for

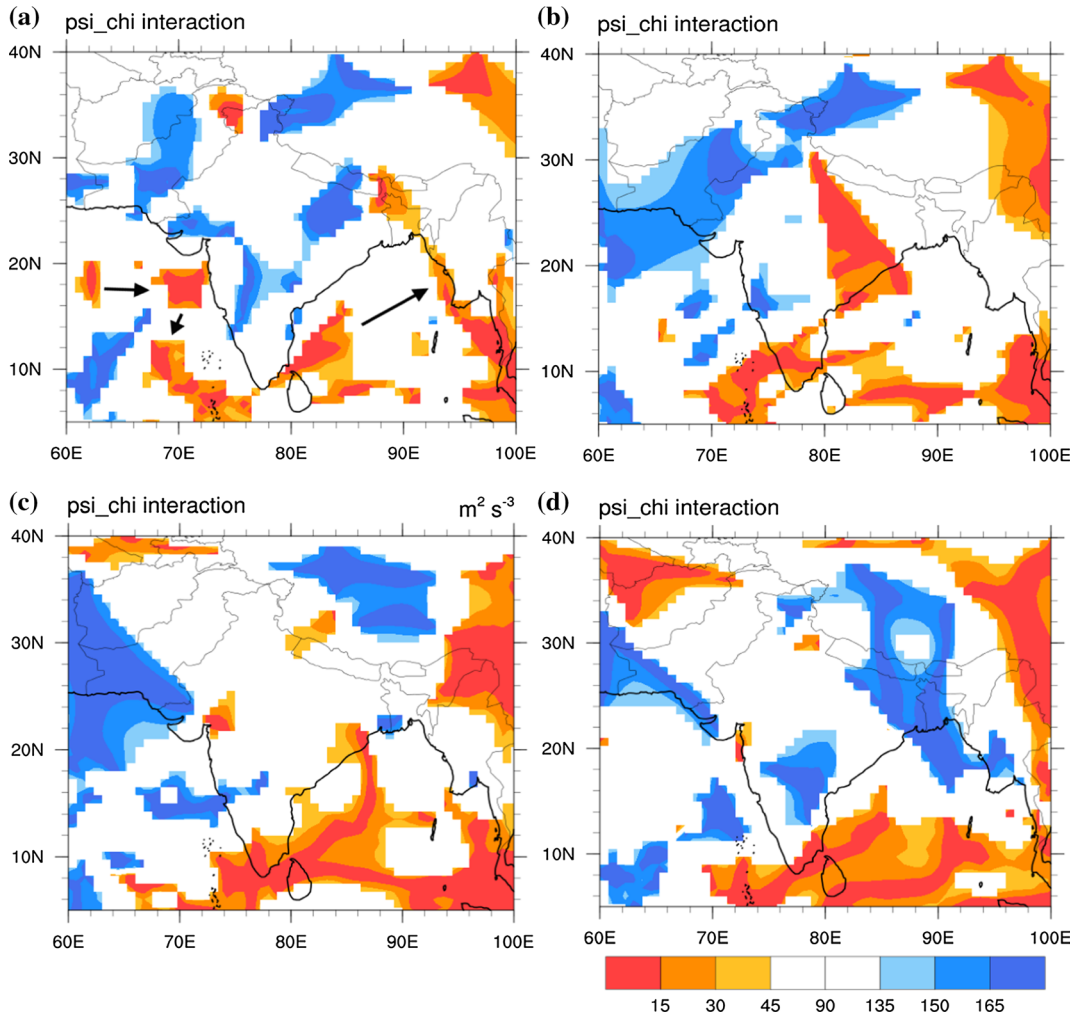

Figure 15. Spatial distribution of angle (x) between $\nabla\psi$ and $\nabla\chi$ vectors at 850 hPa during the (**a**) onset, (**b**) active (composite), (**c**) break (composite), and (**d**) withdrawal phases of monsoon 2014 derived from ERA Interim datasets. The reddish color shows where $0 \leq x \leq 45$, which represents the energy exchange from divergence to rotational kinetic energy and the bluish color shows where $135 \leq x \leq 180$, which represents the rotational kinetic energy losing energy to divergent energy.

2014 summer monsoon. The exchange from the divergent to the rotational kinetic energy for four phases of the monsoon season during 2014 are shown in figure 14(a–d). These illustrations show very striking contrasts among the phases of the monsoon. The onset phase (figure 14a) shows a buildup of the rotational kinetic energy along the west coast of India having much higher magnitude up to 0.004 $m^2\ s^{-3}$. That reddish colouring, for the buildup of the rotational kinetic energy spreads over central and northern India during the active phase of the monsoon (figure 14b) having magnitude as high as up to 0.003 $m^2\ s^{-3}$. The break phase (figure 14c) sees a large spread of very small and negative values all over Indian landmass, i.e., the drop in the rotational kinetic energy of the monsoon as the monsoon weakens. The withdrawal phase (figure 14d), in early September, sees a spread of very small and negative values over most of the central and northern India. Southern tip of India and Sri Lanka starts seeing an enhancement of the rotational kinetic energy in September when the overhead sun has reached 10° north latitude, this is a tag for the start of the winter monsoon.

The spatial distributions of the angle between $\nabla\psi$ and $\nabla\chi$ vectors at 850 hPa level are illustrated in figure 15(a–d). The display here for the exchange from the divergent to the rotational is given by the reddish colour, whereas the converse uses bluish color. During the onset (figure 15a) an anticyclonic circulation is nearly always prevalent over the Arabian Sea (that feature is shown by arrows), the reddish color over south of the Kerala state depicts that where the onset is just

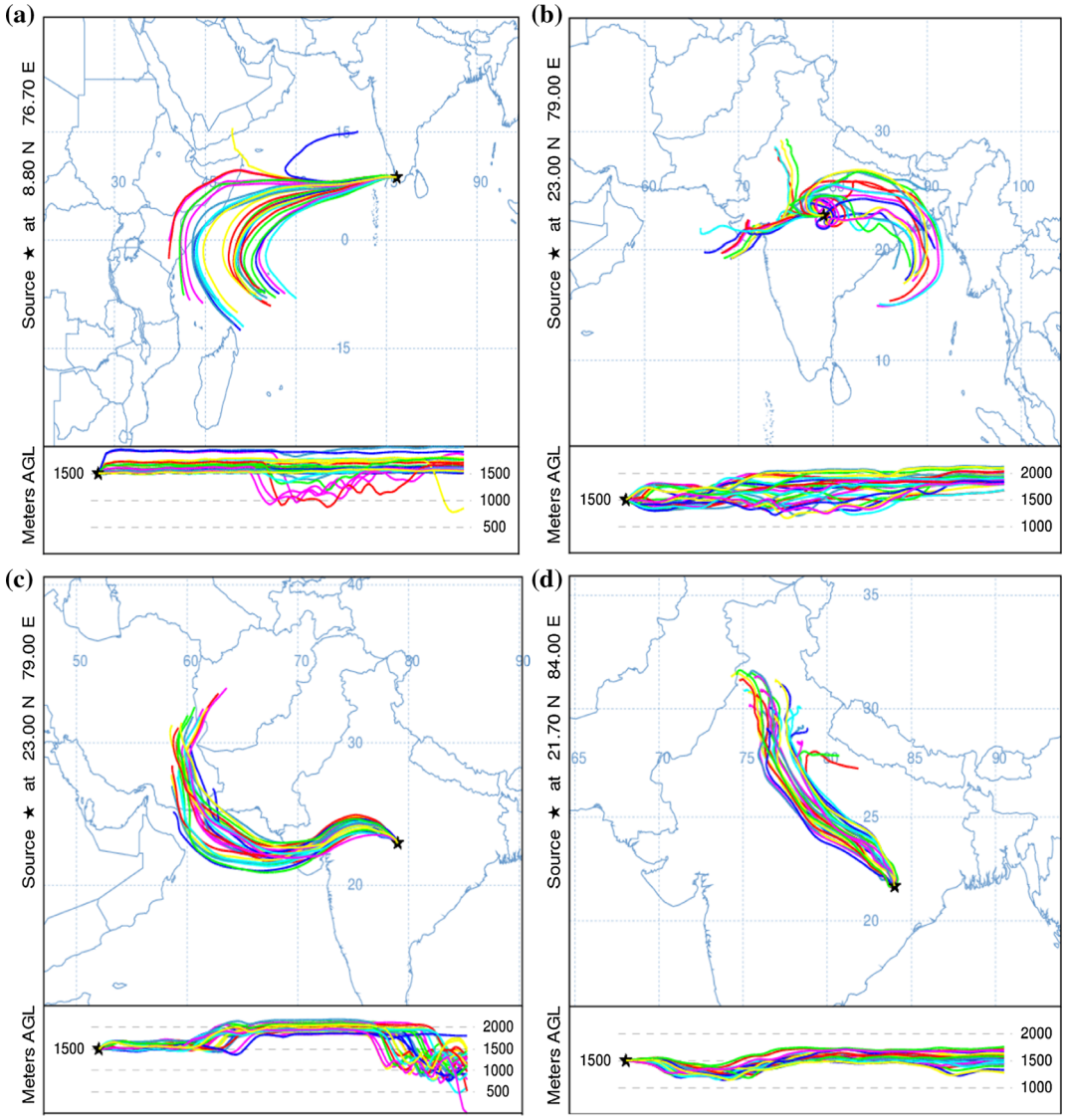

Figure 16. Four-day back trajectories during the (**a**) onset, (**b**) active (composite), (**c**) break (composite), and (**d**) withdrawal phases of monsoon 2014 derived from ERA Interim datasets using the NOAA HYSPLIT computational algorithm.

occurring. During the active phase (figure 15b), the rotational kinetic energy receives energy from the divergent kinetic energy over north central India. The break phase (figure 15c) is characterized by bluish colour implying the rotational kinetic energy is losing energy to the divergent kinetic energy. The withdrawal phase (figure 15d), shows an extension of bluish colour over northeast India that extends into the northern Bay of Bengal. This shows that the velocity potential and the stream function undergo rather fascinating changes during the phases of the monsoon, especially the point by point mutual orientation of the vectors $\nabla\psi$ and $\nabla\chi$. The reddish colour generally implies a strengthening of the monsoon circulation and the bluish colour implies its weakening.

4.8 *Wind trajectories*

We did ask a question, 'Where do parcels, as determined from three-dimensional back trajectories come from, that ended up over India, during the onset, active, break and withdrawal phases of the monsoon'. That is an important philosophical question, since that might provide some clue for the seeming quasi-periodicity of the intra-seasonal behaviour of rains during these phases of the monsoon. These trajectories, based on the NOAA HYSPLIT computational algorithm (Stein *et al.* 2015; Rolph *et al.* 2017), for these transition phases are shown in figure 16(a–d). These illustrations show three dimensional trajectories that terminate at the 1500 m above ground level (AGL) (∼850 hPa level), the inset diagram, within each

panel, carries the height of the parcel. What these shows are the following: During the onset phase over Kerala, the parcels are back tracked to the south-west towards Africa and southward over the Arabian Sea. The active phase invites parcels from both the Arabian Sea and the Bay of Bengal towards central India. The break phase brings in dry air from the deserts to the northwest of India and the northern Arabian Sea. The withdrawal phase brings in north-westerly parcels from north and north-west towards central India.

5. Concluding remarks

This study illustrates the salient cloud structures and atmospheric vertical profiles during the phase transitions of the South Asian summer monsoon from the onset to the withdrawal phase, during the monsoon season of 2014. These findings obtained from the use of diverse satellite products, reanalysis and model datasets, such as precipitation, vertical structures of rain rates, transitions in the dominant cloud types, soil moisture, vertically integrated moisture transports, vertically integrated heat content (i.e., moist static energy), vertical distribution of moisture, circulation features such as the rotational wind, and the divergent wind and the energy exchange from the divergent to the rotational kinetic energy. Sharp transition in these above fields are noted from one phase to the next (such as onset, active, break, revival and the withdrawal phases). A sharp contrast among all these features are seen during the phases. The salient features that are seen here, include the following:

(i) During the transition from an active to a break phase the rainfall intensities over central India go from magnitudes like over 60 mm/day to less than 5 mm/day. These are of course well-known features. Both the TRMM and the GPM carry similar values during these transitions.

(ii) The vertical distributions of clouds from CloudSat, the vertical distribution of rains from TRMM precipitation radar, the vertical structure of radar reflectivity, the vertical profiles of rain, snow, cloud ice and graupel and the dominant cloud types during transitions are very revealing and features that were not mapped during the pre-TRMM/GPM era. The active phase is dominated by rains from nimbostratus, whereas the onset phase sees the much taller cumulonimbus contributing to rather heavy local rains.

(iii) The soil moisture shows a spectacular change from the onset to the active phase; the onset values are akin to a semi-arid land and after the active phase soil moisture increases to values as high as -0.12 to 0.1 m^3/m^3. The break phase, that follows an active phase, does not exhibit a dryness as high as the onset stage because of the high retention of moisture in the soil. The season long rains continue to show fairly high soil moisture during the withdrawal phase.

(iv) The moisture transport vectors (at the 850 hPa level) show rather interesting changes in amplitude and directions of moisture transports, among the ocean basins, during these transitions. The onset phase carries moisture convergence mostly along the west coast of India, whereas during this time the active (or post onset) period of the Myanmar coastal regions and the eastern Bay of Bengal show significant moisture convergence. However, most of central and northern India shows weak to a neutral field of moisture convergence. The active phase stands out carrying a robust field of moisture convergence along central and east coast of India with strong supporting moisture flux from Arabian Sea and Bay of Bengal. During this active phase, a moist stream (moist river) from the central Arabian Sea is clearly seen bringing copious moisture for the heavy rains all along the Western Ghats. In contrast, during the break phase the overall field of moisture convergence is weak and negative over the central and northern India. The withdrawal phase shows a moisture convergence with very weak values over most of India except for the Western Ghats region and the southern tip of India.

(v) The most striking feature in the field of vertically integrated anomaly of the moist static energy is the large built-up of positive values over most of India (especially over central and northern India). Those are important features in our understanding of monsoonal links to regions outside south Asia. Another very striking feature is the wall of moisture that precedes the Kerala Onset (Joshi *et al.* 1990), that moisture in the southern Arabian Sea stand out in the field of moist static energy.

(vi) The evolution of the exchange of energy from the divergent to the rotational kinetic energy has a role in the strengthening of the monsoon circulation and vice versa. The salient contribution for this exchange come from the orientation of the vectors, $\nabla\psi$ and $\nabla\chi$ (Krishnamurti and Ramanathan 1982). During the phase transitions, clearly during the onset phase, the southwest coast of India and the Arabian Sea show large belts where the rotational wind is strengthened by its orientation with respect to the divergent wind. The active phase is characterized by similar large strengthening of the rotational wind over most of Arabian Sea and most parts of India. The break phase shows a rather prominent exchange of rotational kinetic energy towards the divergent kinetic energy over most of central and northern part of South Asia during this weakening phase of the monsoon. During the withdrawal phase there are some transformation of the divergent kinetic energy into rotational kinetic energy over south of Tamil Nadu and Sri Lanka, those features are associated with the withdrawal of south-west monsoon circulations.

(vii) We noted a strong positive relationship between the rainfall totals during the phases of the monsoon and the domain averaged moisture convergence over central India. This simply states that the intra-seasonal rainfall variability relates rather closely to the moisture convergence. These results are also confirmed by the band pass filtered 850 hPa level winds over India that show the passage of ISO and show the passage of alternating parallel and antiparallel anomalies, on the ISO time scale. These features strengthen and weaken the monsoon during the phases.

(viii) The information from trajectories itself does not provide any answer to the quasi-periodicity of the intra-seasonal behaviour of rains over central India. The varying structures of the atmosphere during the different phases, as portrayed in this study, are not adequate to explain why we have this quasi-periodicity on the time scale of ISO. That more fundamental question must be tied to basic large-scale instability (linear or more likely nonlinear, in space and time) that invites outside air to behave in the way it does. A second part of this study examines the relationship between monsoon rains of the intra-seasonal time scale and remote factors.

Acknowledgements

This work was supported by the research grant from NASA/PMM grant No. NNX16AD83G. The authors gratefully acknowledge NASA for TRMM, GPM/IMERG and CloudSat products and NCEP/NCAR for providing the GFS data for model simulation. We are thankful to Prof. Vasu Misra, Department of Earth, Ocean and Atmospheric Science, Florida State University for his feedback and helpful discussions to improve this manuscript. We also thank the anonymous reviewers for their valuable comments and suggestions.

Appendix

The vertically integrated moisture transport vectors and convergence of flux of moisture (MFC) transport are estimated from the following formulations:

$$\overrightarrow{M_x} = -\frac{1}{g}\int_{Psuf}^{Ptop} \vec{U} q \; dp,$$

is the total column zonal flux of moisture.

$$\overrightarrow{M_y} = -\frac{1}{g}\int_{Psuf}^{Ptop} \vec{V} q \; dp,$$

is the total column meridional flux of moisture.

$$\vec{M} = i \cdot \overrightarrow{M_x} + j \cdot \overrightarrow{M_y},$$

representation of vertically integrated moisture transport vector.

$$MFC = (-1) * \vec{\nabla} \cdot \vec{M},$$

convergence of vertically integrated moisture transport.

Here, g is the acceleration due to gravity, $\vec{U}$ and $\vec{V}$ are the zonal and meridional wind components, $\vec{\nabla}$ is the del operator, and q, the moisture parameter.

References

Bounoua L and Krishnamurti T N 1993 Influence of soil moisture on the Sahelian climate prediction I; *Meteorol. Atmos. Phys.* **52** 183–203.

Cadet D L and Greco S 1987a Water vapor transport over the Indian Ocean during the 1979 summer monsoon. Part I: Water vapor fluxes; *Mon. Weather Rev.* **115** 653–663.

Cadet D L and Greco S 1987b Water vapor transport over the Indian Ocean during the 1979 summer monsoon. Part II: Water vapor Budgets; *Mon. Weather Rev.* **115** 2358–2366.

Chakraborty A and Nanjundiah R S 2012 Space–time scales of northward propagation of convection during boreal summer; *Mon. Weather Rev.* **140** 3857–3866.

Dee D P *et al.* 2011 The ERA-Interim reanalysis: Configuration and performance of the data assimilation system; *Q. J. Roy. Meteor. Soc.* **137** 553–597.

Deshpande N R and Goswami B N 2014 Modulation of the diurnal cycle of rainfall over India by intraseasonal variations of Indian summer monsoon; *Int. J. Climatol.* **34** 793–807.

Dudhia J 1989 Numerical study of convection observed during the Winter Monsoon Experiment using a mesoscale two-dimensional model; *J. Atmos. Sci.* **46** 3077–3107.

Hazra A, Chaudhari H S, Saha S K and Pokhrel S 2017 Effect of cloud microphysics on Indian summer monsoon precipitating clouds: A coupled climate modeling study; *J. Geophys. Res. Atmos.* **122** 3786–3805, https://doi.org/10.1002/2016jd026106.

Hong Song-You, Yign Noh and Jimy Dudhia 2006 A new vertical diffusion package with an explicit treatment of entrainment processes; *Mon. Weather Rev.* **134** 2318–2341.

Huffman G J *et al.* 2007 The TRMM Multi satellite Precipitation Analysis: Quasi-global, multiyear, combined-sensor precipitation estimates at fine scale; *J. Hydrometeor.* **8** 38–55, https://doi.org/10.1175/jhm560.1.

Huffman G J, Adler R F, Bolvin D T and Nelkin E J 2010 The TRMM Multi-Satellite Precipitation Analysis (TMPA); In: *Satellite Rainfall Applications for Surface Hydrology* (eds) Hossain F and Gebremichael M, Springer, pp. 3–22.

Huffman G J *et al.* 2015a NASA Global Precipitation Measurement (GPM) Integrated Multi-satellitE Retrievals for GPM (IMERG). Algorithm Theoretical Basis Doc., version 4.5, 26p., http://pmm.nasa.gov/sites/default/files/document_files/IMERG_ATBD_V4.5.pdf.

Huffman G J, Bolvin D T and Nelkin E J 2015b Integrated Multi-satellitE Retrievals for GPM (IMERG) technical documentation; NASA Doc., 47p., http://pmm.nasa.gov/sites/default/files/document_files/ IMERG_doc.pdf.

Janowiak J E, Joyce R J and Yarosh Y 2001 A real-time global half-hourly pixel-resolution infrared dataset and its applications; *Bull. Am. Meteor. Soc.* **82** 205–217, https://doi.org/10.1175/1520-0477(2001)082,0205:artghh.2.3.co;2.

Joshi P C, Simon B and Desai P S 1990 Atmospheric thermal changes over the Indian Ocean using satellite data, physical processes in atmospheric models; *Int. J. Climatol.* **10** 49–56.

Kain J S and Fritsch J M 1993 Convective parameterization for mesoscale models: the Kain–Fritsch scheme; In: *The Representation of Cumulus Convection in Numerical Models* (eds) Emanuel K A and Raymond D J, chap. 16, vol. 24, AMS Press, Boston.

Kiran R V, Rajeevan M, Rao S V B and Prabhakara Rao N 2009 Analysis of variations of cloud and aerosol properties associated with active and break spells of Indian summer monsoon using MODIS data, *Geophys. Res. Lett.* **36** L09706, https://doi.org/10.1029/2008gl037135.

Krishnamurti T N, Kumar V, Simon A, Thomas A, Bhardwaj A, Das S, Senroy S and Roy Bhowmik S K 2016 March of buoyancy elements during extreme rainfall over India; *Clim. Dyn.* **48(5)** 1931–1951.

Krishnamurti T N and Biswas M K 2006 Transitions in the surface energy balance during the life cycle of a monsoon season*; J. Earth Syst. Sci.* **115(2)** 185–201.

Krishnamurti T N, Bedi H S, Hardiker V and Watson-Ramaswamy L 2006 *An Introduction to Global Spectral Modeling*; Oxford University Press, Springer, New York, Chap. 10, 213–251, https://doi.org/10.1007/0-387-32962-5.

Krishnamurti T N and Kishtawal C M 2000 A pronounced continental-scale diurnal mode of the Asian summer monsoon. *Mon. Weather Rev.* **128** 462–473.

Krishnamurti T N and Subrahmanyam D 1982 The 30–50 day mode at 850 hPa during MONEX; *J. Atmos. Sci.* **39** 2088–2095.

Krishnamurti T N and Ramanathan Y 1982 Sensitivity of the monsoon onset to differential heating; *J. Atmos. Sci.* **39** 1290–1306.

Krishnamurti T N, Ardanuy P, Ramanathan Y and Pasch R 1981 On the onset vortex of the summer monsoon; *Mon. Weather Rev.* **109** 344–363.

Kulkarni A, Kripalani R, Sabade S and Rajeevan M 2011 Role of intra-seasonal oscillations in modulating Indian summer monsoon rainfall; *Clim. Dyn.* **36** 1005–1021.

Lin Y-L, Rareley R D and Orville H D 1983 Bulk parameterization of the snow field in a cloud model; *J. Appl. Meteor.* **22** 1065–1092.

Liu Z 2015 Comparison of Integrated multisatellite retrievals for GPM (IMERG) and TRMM multisatellite precipitation analysis (TMPA) monthly precipitation products: Initial results; *J. Hydrometeor.* **17** 777–790.

Mlawer E J, Taubman S J, Brown P D, Iacono M J and Clough S A 1997 Radiative transfer for inhomogeneous atmosphere: RRTM, a validated correlated-k model for the longwave; *J. Geophys. Res.* **102** 16,663–16,682.

Nakagawa K, Yoshida N and Higashiuwatoko T 2011 PR V7 2A25 evaluation using the conventional radar in Japan; TRMM Doc., JAXA, 11p.

Neeck S P, Kakar R, Azarbarzin A, Hou A and Skofronick-Jackson G 2014 Global Precipitation Measurement (GPM) Launch, Commissioning, and Early Operations. Sensors, Systems, and Next-Generation Satellites XVIII Book Series; *Proc. SPIE*, https://doi.org/10.1117/12.2069868.

Pillai P A and Sahai A K 2014 Moist dynamics of active/break cycle of Indian summer monsoon rainfall from NCEPR2 and MERRA reanalysis; *Int. J. Climatol.* **34** 1429–1444.

Rajeevan M, Bhate J, Kale J D and Lal B 2005 Development of a high resolution daily gridded rainfall data for the Indian region. *Met. Monogr. Climatol.* **22** 2005.

Rajeevan M, Gadgil S and Bhate J J 2010 Active and break spells of the Indian summer monsoon; *J. Earth Syst. Sci.* **119** 229–247.

Rao Y P 1976 *Meteorological Monograph Synoptic Meteorology No. 1/1976*, Southwest Monsoon, India Meteorological Department.

Revadekar J V, Kumar K R, Tiwari Y K and Valsala V 2016 Variability in AIRS CO_2 during active and break phases of Indian summer monsoon; *Sci. Total Environ.* **541** 1200–1207.

Roja Raman M, Jagannadha Rao V V M, Venkat Ratnam M, Kishore Kumar G, Narendra Babu A, Vijaya Bhaskara Rao

S, Prabhakara Rao N and Narayana Rao D 2008 Atmospheric circulation during active and break phases of Indian summer monsoon: A study using MST radar at Gadanki (13.5°N, 79.2°E); *J. Geophys. Res.* **113** D20124, https://doi.org/10.1029/2008jd010341.

Rolph G, Stein A and Stunder B 2017 Real-time Environmental Applications and Display sYstem: READY; *Environ. Model. Softw.* **95** 210–228, https://doi.org/10.1016/j.envsoft.2017.06.025.

Sahu D K, Dash S K and Bhan S C 2014 Impact of surface observations on simulation of rainfall over NCR Delhi using regional background error statistics in WRF-3DVAR model; *Meteorol. Atmos. Phys.* **125** 17–42, https://doi.org/10.1007/s00703-014-0320-x.

Simpson J, Kummerow C, Tao W K and Adler R F 1996 On the tropical rainfall measuring mission (TRMM); *Meteorol. Atmos. Phys.* **60** 19–36.

Stein A F, Draxler R R, Rolph G D, Stunder B J B, Cohen M D and Ngan F 2015 NOAA's HYSPLIT atmospheric transport and dispersion modeling system, *Bull. Am. Meteor. Soc.* **96** 2059–2077, https://doi.org/10.1175/BAMS-D-14-00110.1.

Stephens G L *et al.* 2002 The CloudSat mission and the A-Train: A new dimension of space-based observations of clouds and precipitation; *Bull. Am. Meteor. Soc.* **83(12)** 1771–1790.

Tao W-K *et al.* 2009 Goddard multi-scale modeling systems with unified physics; *Ann. Geophys.* **27** 3055–3064.

Tao W-K, Wu D, Lang S, Chern J-D, Peters-Lidard C, Fridlind A and Matsui T 2016 High-resolution NU-WRF simulations of a deep convective-precipitation system during MC3E: Further improvements and comparisons between Goddard microphysics schemes and observations; *J. Geophys. Res. Atmos.* **121** 1278–1305, https://doi.org/10.1002/2015jd023986.

Waliser D E 2006 Intra-seasonal variability; In: *The Asian Monsoon* (ed.) Bin Wang, Ch. 5, pp. 203–257.

Waliser D E, Stern W, Schubert S and Lau K M 2003 Dynamic predictability of intraseasonal variability associated with the Asian summer monsoon; *Q. J. Roy. Meteorol. Soc.* **129** 2897–2925.

Wonsick M M, Pinker R T and Govaerts Y 2009 Cloud variability over the Indian monsoon region as observed from satellites; *J. Appl. Meteor. Climatol.* **48** 1803–1821.

Corresponding editor: N V Chalapathi Rao